

Modeling the elastic transmission of tidal stresses to great distances

J. Thompson et al.

Modeling the elastic transmission of tidal stresses to great distances inland in channelized ice streams

J. Thompson, M. Simons, and V. C. Tsai

Seismological Laboratory, Division of Geological and Planetary Sciences, California Institute of Technology, MC 252-21, 1200 E. California Blvd., Pasadena, CA 91125

Received: 21 February 2014 – Accepted: 11 March 2014 – Published: 25 April 2014

Correspondence to: J. Thompson (jeffremt@gmail.com)

Published by Copernicus Publications on behalf of the European Geosciences Union.

Title Page

Abstract

Introduction

Conclusions

References

Tables

Figures

⏪

⏩

◀

▶

Back

Close

Full Screen / Esc

Printer-friendly Version

Interactive Discussion

Abstract

Geodetic surveys suggest that ocean tides can modulate the motion of Antarctic ice streams. Data from Whillans Ice Plain, Rutford Ice Stream, and other Antarctic ice streams show periodicity in flow velocity at periods similar to those of ocean tides at geodetic stations many tens of kilometers inland from the grounding line. These data suggest that ocean tidal stresses can perturb ice stream motion at distances about an order of magnitude farther inland than tidal flexure of the ice stream alone. Recent models exploring the role of tidal perturbations in basal shear stress are primarily two-dimensional, with the impact of the ice stream margins either ignored or parameterized. Here, we use two- and three-dimensional finite element modeling to investigate transmission of tidal stresses in ice streams and the impact of considering more realistic, three-dimensional ice stream geometries. Using Rutford Ice Stream as a real-world comparison, we demonstrate that the assumption that elastic tidal stresses in ice streams propagate large distances inland fails for channelized glaciers due to an intrinsic, exponential decay in the stress due to resistance at the ice stream margins. This behavior is independent of basal conditions beneath the ice stream and cannot be fit to observations using either elastic or nonlinear viscoelastic rheologies without nearly complete decoupling of the ice stream from its lateral margins. Our results suggest that a mechanism external to the ice stream is necessary to explain the tidal modulation of stresses far upstream of the grounding line for narrow ice streams. We propose a hydrologic model based on time-dependent variability in till strength to explain transmission of tidal stresses inland of the grounding line. This conceptual model reproduces observations from Rutford Ice Stream.

Modeling the elastic transmission of tidal stresses to great distances

J. Thompson et al.

Title Page

Abstract

Introduction

Conclusions

References

Tables

Figures



Back

Close

Full Screen / Esc

Printer-friendly Version

Interactive Discussion



1.2 Previous relevant modeling

Many models have been proposed to explain the influence that ocean tides have on the motion of some Antarctic ice streams (e.g., Anandakrishnan and Alley, 1997; Bind-
schadler et al., 2003; Gudmundsson, 2006, 2007, 2011; Sergienko et al., 2009; Walker
et al., 2012; Winberry et al., 2009). Given that the Maxwell relaxation time for ice is
on the order of hours for tidal loads, these models call on either elastic or viscoelastic
transmission of tidal loading stresses through the ice stream to drive the observed ice
motions.

We discuss several representative published models to highlight the assumptions
made about the upstream transmission of tidal stress. A flow-line model assumes that
all transverse stresses are negligible, reducing the glacier model to a two-dimensional
cross section. A flow-line model for an ice stream, governed by the assumption that
a weak frictional resistance supports any tidal loading, is only appropriate far from the
lateral margins of an ice stream such that any resistance from these margins can be
neglected. When simplified into one dimension, such a model reduces to the spatially
averaged shear stress formulation of Bind-schadler et al. (2003) and Winberry et al.
(2009). These models assume that tidal stress is uniformly distributed over the entire
ice stream, being completely supported by the ice stream's base. The result is that
the length-scale of the transmission of stress depends completely on the length and/or
thickness of the ice stream assumed in the problem.

Finite element analysis in two-dimensions allows for flow-line models with increased
complexity and realistic geometries. The two most applicable models of tidal stress
propagation are those of Gudmundsson (2011) and Walker et al. (2012). Both are two-
dimensional flow-line models incorporating nonlinear viscoelasticity and a nonlinear
basal sliding law. In these analyses, the response of the modeled ice stream relates
directly to the basal boundary condition. This result is intuitive as any resistance due
to the lateral margins of the ice is neglected (being a flow-line model) and thus the
model ice stream's response to a tidal load can only be controlled by assumed rheo-

Modeling the elastic transmission of tidal stresses to great distances

J. Thompson et al.

Title Page

Abstract

Introduction

Conclusions

References

Tables

Figures

⏪

⏩

◀

▶

Back

Close

Full Screen / Esc

Printer-friendly Version

Interactive Discussion



logical character of the stream's bed alone. These models are attractive as the basal rheologies can be tuned to accurately match observations. However, the fact that these models can be made to fit the observations does not demonstrate that the lateral resistance in these ice streams is indeed negligible. Note that a three-dimensional version of Gudmundsson's model is currently in review and is publically available online for viewing (Rosier et al., 2014).

Alternatively, Sergienko et al. (2009) approximated an ice stream as a series of masses (blocks) connected elastically (by springs) and restrained laterally (by further springs) with a shear stress applied along a frictional basal contact. Unlike the flow-line models, this spring-block model incorporates the lateral resistance of the ice margins. Sergienko et al. (2009) note that a "tidal" load applied at one edge in this model diminishes with distance from the loaded block, but this stress decay is not explored in further detail. We assume that this distance depends on the stiffness of the springs, both between the masses and as lateral restraints, as well as the magnitude of the basal friction imposed in the model. However, there is no obvious relation between a physical length scale and the number of blocks and springs in the model, and it is not clear if the decay of the tidal stress is caused by marginal or basal resistance.

2 Methodology

We present results from two-dimensional (2-D) and three-dimensional (3-D) elastic and viscoelastic models that explore the role that ice stream geometry plays in controlling transmission of tidal stresses. We describe our models below and show them schematically in Fig. 2.

We begin with a two-dimensional elastic flow-line model (Fig. 2a) using finite-elements both to benchmark the computational models and to determine the expected range of stress transmission for the modeled ice stream. As with all flow-line models, the underlying assumption is that the ice stream is infinite and uniform in the third dimension, such that there effectively are no lateral margins to the ice stream. These

Modeling the elastic transmission of tidal stresses to great distances

J. Thompson et al.

Title Page

Abstract

Introduction

Conclusions

References

Tables

Figures



Back

Close

Full Screen / Esc

Printer-friendly Version

Interactive Discussion



simplified models allow us to establish “end member” behaviors of an elastic ice stream with the extreme basal conditions of either a fully frozen (no slip) or a freely sliding (no shear traction) bed. Additionally, we use these 2-D models to investigate the role played by an ice shelf as an intermediary between the ocean tides and the grounded ice stream (see Appendix A).

Based on the intuition gained from these 2-D models, we then explore a series of 3-D models (Fig. 2b) to study the impact of resistive shearing at the lateral margins of the model on the upstream transmission of an applied tidal load. We first investigate the role that the overall geometry of the ice stream (i.e. ice stream width and thickness) has on the transmission of tidal stresses inland of the grounding line. From these models, we find that including the lateral margins of the ice stream inherently limits the inland distances to which tidal stress are transmitted to values too small to be consistent with observations, even in the case of frictionless sliding at the bed.

In the second part of this paper, we consider two physically-motivated mechanisms for decoupling the model ice stream from its lateral margins. First, we consider a model with more compliant ice in the margins to investigate the role that “weakened” ice in the margins may have on stress transmission. Second, we modify the rheological model to a Glen-style viscoelastic constitutive law to investigate the role that viscoelasticity may play in the transmission of tidal stresses inland of the grounding line.

We compare the modeling results to tidally-modulated GPS data from Rutford Ice Stream, finding that we cannot match observations using a model based around the transmission of a tidal load through an ice stream’s bulk. We close with a hydrological model that demonstrates that the transmission of tidal information far inland of an ice stream’s grounding line can occur through a process external to the ice stream itself.

2.1 Model construction

Our calculations rely on the finite element analysis software *PyLith* (Aagaard, 2013a, b) for our numerical modeling. This open-source Lagrangian FEM code has been developed and extensively benchmarked in the crustal deformation community (available

TCD

8, 2119–2177, 2014

Modeling the elastic transmission of tidal stresses to great distances

J. Thompson et al.

Title Page

Abstract

Introduction

Conclusions

References

Tables

Figures

⏪

⏩

◀

▶

Back

Close

Full Screen / Esc

Printer-friendly Version

Interactive Discussion



at www.geodynamics.org/cig/software/pylith). *PyLith* solves the conservation of momentum equations with an associated rheological model. As we assume a quasistatic formulation (i.e., all inertial terms are dropped), the governing equations are:

$$\begin{aligned} \sigma_{ij,j} &= f_i & \text{in } V \\ \sigma_{ij}n_j &= T_i & \text{on } S_T \\ u_i &= u_i^0 & \text{on } S_U \end{aligned} \quad (1)$$

where V is an arbitrary body with boundary condition surfaces on S_T and S_U . On S_T , the traction $\sigma_{ij}n_j$ equals the applied Neumann boundary condition T_i . On S_U , the displacement u_i is set equal to the applied Dirichlet boundary condition u_i^0 .

PyLith solves these equations using a Galerkin formulation of the spatial equation and an unconditionally stable method of implicit time-stepping for both an elastic and viscoelastic rheology (following the form of Bathe, 1995). For model convergence, we select a tolerance of 10^{-12} in the absolute residual of the iterative solver from the *PETSc* library (Balay et. al 1997, 2012a, b) and a relative tolerance to the initial residual value of 10^{-8} . Based on several experiments, these values are sufficiently conservative to ensure solution convergence without causing a prohibitive increase in computational time.

Due to the superposition property of a linear elastic model, we choose to neglect the effect of gravity as a body force, setting f_i equal to 0, effectively neglecting the background flow of the ice stream. For the nonlinear viscoelastic models, we cannot use superposition and thus we apply the down-glacier component of the gravitational body force, equal to $g \sin \alpha$ where α is the surface slope. We choose to apply only the down-glacier component of gravity out of convenience, as a using the full gravitational body force would require us to apply a pre-stress to the model cancel out the vertical component of the full gravitational body force anyways, or the model would compress when gravity was “turned on” at time 0.

Our basal boundary condition is either a Dirichlet condition with zero-displacement in all directions (“frozen”) or a free-slip condition with no vertical displacements and zero

Modeling the elastic transmission of tidal stresses to great distances

J. Thompson et al.

Title Page	
Abstract	Introduction
Conclusions	References
Tables	Figures
⏪	⏩
◀	▶
Back	Close
Full Screen / Esc	
Printer-friendly Version	
Interactive Discussion	



known for ice (and thus is fixed) when exploring the ranges in values of the other elastic moduli. We also consider a Glen-style Maxwell viscoelastic rheology:

$$\dot{\epsilon} = \frac{\dot{\sigma}}{E} + A\sigma^n \quad (3)$$

5 where we take the canonical value $n = 3$. For the viscosity coefficient A , we present two models. The first is a homogenous viscous model, using the canonical value of A equal to the 0°C value (e.g. Cuffey and Paterson, 2010). The second model uses the Arrhenius relationship for temperature-dependent viscosity from Cuffey and Paterson (2010, Eq. 3.35), along with a temperature profile chosen to match the empirical rela-
10 tion calculated from the Whillans Ice Plain in Engelhardt and Kamb (1993). The elastic moduli are the same as in the homogenous elastic models.

3 Results

Our finite element formulation calculates the full stress and strain tensors, as well as displacement and velocity vectors at every node of the model mesh. While we ran
15 close to forty models, we only show representative figures (Figs. 3, 4, 6, 8, 10, and 11); however, we present tabulated results from all models (in Tables 4–6). To aid in comparing the magnitude of stress between models, we define an equivalent stress, τ_{eq} , based on the Von Mises criterion. τ_{eq} is defined in 2-D and 3-D as:

$$\text{2-D: } \tau_{\text{eq}}^2 = \frac{1}{2} \left[(\sigma_{xx} - \sigma_{yy})^2 + \sigma_{xx}^2 + \sigma_{yy}^2 + 6\sigma_{xy}^2 \right] \quad (4a)$$

$$\text{20 3-D: } \tau_{\text{eq}}^2 = \frac{1}{2} \left[(\sigma_{xx} - \sigma_{yy})^2 + (\sigma_{yy} - \sigma_{zz})^2 + (\sigma_{xx} - \sigma_{zz})^2 + 6 \left(\sigma_{xy}^2 + \sigma_{yz}^2 + \sigma_{xz}^2 \right) \right] \quad (4b)$$

3.1 Two-dimensional results

First, we consider the distribution of stress from the 2-D models with free sliding and frozen basal boundary conditions – shown in Figs. 3 and 4, respectively. We show

Modeling the elastic transmission of tidal stresses to great distances

J. Thompson et al.

Title Page

Abstract

Introduction

Conclusions

References

Tables

Figures

⏪

⏩

◀

▶

Back

Close

Full Screen / Esc

Printer-friendly Version

Interactive Discussion

as the stresses decay with distance inland of the grounding line. Figure 6 shows the full basal stress field of a representative 3-D uniform model using the six independent stress components. The longitudinal normal stresses (σ_{xx}), transverse normal stresses (σ_{yy}), and the shear due to the sidewalls (σ_{xy}) are the largest stresses beyond a few kilometers inland of the forced edge. The vertical normal stress (σ_{zz}) at the bed is also nonzero inland of the forced edge but is at least an order of magnitude smaller than the aforementioned stresses. The other shear stress components (σ_{xz} and σ_{yz}) are direct consequences of stress concentration at the transition from sliding to frozen ice at the base, and decay rapidly with distance from both the margins and the grounding line.

3.3 Geometric factors influencing the transmission of tidal stresses

As seen in models with a resistance at a boundary, stresses resulting from tidal loading decay exponentially with distance inland of the grounding line. We use L_{tr} as a direct measure of the distance that a tidal load influences the motion of an ice stream. Note that we generally estimate L_{tr} using τ_{eq} as this definition of L_{tr} matches the longest L_{tr} of the individual stress components (see Table 3) while allowing us to have a single parameter to compare between models.

To determine the influence that the choice of geometry, form of loading, and value of elastic moduli play in controlling L_{tr} , we explore models varying these three parameters, assuming homogenous elasticity. L_{tr} for many different combinations of these parameters are tabulated in Table 4 for the 2-D models and in Table 5 for the 3-D models.

In all models, stresses vary linearly with the magnitude of the applied load, while displacements vary proportionally to the applied load and the inversely to the Young's modulus. Such results are expected from linear elasticity. However, neither of these parameters has any effect on the nature of the stress decay (as evidenced by the nearly constant L_{tr}).

Modifying the geometry of the model ice streams affects the value of the stresses and displacements throughout the model in a nonlinear fashion, due to the differences

in distance from the fixed and forced edges in the model. The choice of geometry also impacts the value of L_{tr} . For the 2-D models (with a frozen bed), L_{tr} varies linearly with thickness. For the 3-D models, L_{tr} increases with increasing thickness and width, but not in a strictly linear fashion for either.

5 Given the geometric dependencies described above, we find that the following empirical functional forms describe the relationship between the stresses, displacements, and model parameters very well. For the 2-D model, we use:

$$\begin{aligned}\sigma(x, z) &= \sigma_{GL}(h, z) \cdot \Delta\bar{h} \cdot 10^{-x \frac{\bar{h}}{L_{tr}}} \\ u(x, z) &= u_{GL}(h, z) \cdot \frac{\Delta\bar{h}}{\bar{E}} \cdot 10^{-x \frac{\bar{h}}{L_{tr}}}\end{aligned}\quad (5)$$

10 Where σ_{GL} and u_{GL} are respectively the stress and displacement at the grounding line for a 1 km-thick model with a one meter tidal load using the canonical value of 9.8 GPa for E , \bar{E} is the non-dimensionalized Young's modulus with respect to the canonical value, \bar{h} is the non-dimensionalized model thickness with respect to a 1 km reference value, and $\Delta\bar{h}$ is the non-dimensionalized tidal height with respect to a 1 m tide. For the
15 3-D models, we adopt the functional forms:

$$\begin{aligned}\sigma(x, y, z) &= \sigma_{GL}(y, z, h, w) \cdot \Delta\bar{h} \cdot 10^{-x \frac{\bar{h}}{L_{tr}(h, w)}} \\ u(x, y, z) &= u_{GL}(y, z, h, w) \cdot \frac{\Delta\bar{h}}{\bar{E}} \cdot 10^{-x \frac{\bar{h}}{L_{tr}(h, w)}}\end{aligned}\quad (6)$$

The implications of these results are that the stress distributions depend only on model loading and geometry, and are independent of the elastic properties in the model as
20 long as we assume homogenous elasticity (this second conclusion is not true for models with spatially variable elastic moduli, as discussed in the next section).

From Table 5, we see that L_{tr} is roughly between 1.2 and 1.5 times the ice stream full width and only increases slightly with increasing ice stream thickness in the 3-D

Modeling the elastic transmission of tidal stresses to great distances

J. Thompson et al.

Title Page	
Abstract	Introduction
Conclusions	References
Tables	Figures
⏪	⏩
◀	▶
Back	Close
Full Screen / Esc	
Printer-friendly Version	
Interactive Discussion	



Modeling the elastic transmission of tidal stresses to great distances

J. Thompson et al.

Title Page

Abstract

Introduction

Conclusions

References

Tables

Figures

⏪

⏩

◀

▶

Back

Close

Full Screen / Esc

Printer-friendly Version

Interactive Discussion



models. Thus, tidal stresses at a distance equivalent to two ice stream widths inland of the grounding line should be considerably reduced. Real ice streams are obviously neither frozen nor sliding frictionlessly over their beds; frictional sliding plays a major role in determining the ice stream's total flow (e.g., Weertman, 1957, 1964; Engelhardt and Kamb, 1998; Hughes, 1998; Cuffey and Paterson, 2010). However, as we assume frictionless sliding, the values of L_{tr} for the 3-D models should be taken as maximum values and thus moving to a frictional model would only serve to reduce L_{tr} . Thus, these models imply that the motion of a channelized elastic ice stream should not be tidally-modulated farther inland than about two ice widths from the grounding line – a result contrary to observations of Gudmundsson (2006, 2007, 2011) from Rutford Ice Stream (as shown in Fig. 7a). Given the important role of marginal support of any given ice stream, we also consider potential mechanisms for decoupling the ice stream from its lateral margins, thus increasing the length-scale for the transmission of a tidal stress.

4 Weakening in the ice stream margins

In the previous section, we demonstrated that the resistance from the shear margins of a channelized ice stream damps the tidal stresses significantly and that decay of tidal stresses is independent of the Young's modulus for the case of a homogenous medium. However, as shear margins are locations of enhanced viscous flow (e.g., Dahl-Jensen and Gundestrup, 1987; Echelmeyer and Zhongxiang, 1987; Paterson, 1991; Echelmeyer et al., 1994) as well as crevassing, it is conceivable that ice stream margins are elastically more compliant than the central portion of the ice stream. We now investigate the potential impact that such marginal compliance has on the transmission of tidal stress.

Theoretically, the presence of damage is expected to reduce the ice's effective Young's modulus (e.g., Walsh, 1965). We parameterize the influence of cracks and crevasses using linear elastic continuum damage mechanics. Such a mechanism directly modifies the elastic modulus, mapping directly into the linear elastic constitutive

equation as (please see Murakami, 2012 and references therein):

$$\varepsilon = \frac{\sigma}{E(1-D)} \quad (7)$$

The damage parameter D can take a value between 0 (no damage) to 1 (complete plastic failure), and has the physical interpretation as the fraction of area that can no longer support a load due to the opening of void space in the damaged body. For reference, Borstad et al. (2012) find the threshold for calving in the ice shelf to be $D = 0.6 \pm 0.1$, similar to the value of damage calculated from viscous flow enhancement factors for an Antarctic ice stream (e.g., Echelmeyer and other, 1994) using a viscous implementation of damage (see Eq. (8) below). Our modeling, described below, suggests that to match observed stress transmission length-scales requires damage in the marginal ice sufficient to reduce the outer Young's modulus (E_L) to between 10 and 1000 times more compliant than the central ice (E_H).

We modify our 3-D model to have a laterally variable Young's modulus with two different patterns of variability (see inset in Fig. 2b): one with a step function drop in Young's modulus at certain predetermined ice margin widths ("discrete margins") and another with a linear reduction of the Young's modulus from the middle of the ice stream to the edge of the stream ice ("continuous margins"). For the latter margin pattern, we evaluate a range of margin widths at 10% intervals between 10% and 90% of the ice stream half-width. Also note that in models with discrete margins, we only model a reduction in modulus by a factor of 10.

Figure 8 shows a representative distribution of the six stress components for the discrete margin model with ice margins chosen to be 1/4 of the ice stream width. The longitudinal normal stress (σ_{xx}) is concentrated in the stronger ice at the center of the model, while the transverse normal (σ_{yy}) and the horizontal shear (σ_{xy}) stresses are concentrated in the weaker marginal ice. Comparing the stresses in Fig. 6, and noting the differing longitudinal scales, it is clear that L_{tr} is larger in the model with compliant margins than the homogenous elastic model. Additionally, as shown for the longitudinal normal stress (σ_{xx}), L_{tr} is no longer constant throughout the model, as was the case

Modeling the elastic transmission of tidal stresses to great distances

J. Thompson et al.

Title Page

Abstract

Introduction

Conclusions

References

Tables

Figures

⏪

⏩

◀

▶

Back

Close

Full Screen / Esc

Printer-friendly Version

Interactive Discussion



for a uniform model. We use a width-averaged value of L_{tr} for comparison between different models.

Figure 9 shows the modeled increase in L_{tr} relative to a uniform model as a function of margin-widths and marginal damage parameter. Note that we base the margin-width relationship based on the discrete margins models while we use the continuous margins models to characterize the marginal damage relationship. Figure 9 demonstrates that the maximum increase to L_{tr} occurs when the shear margins are about 50 % of the ice stream half-width (25 % of the ice stream full-width) and when the lateral margins are substantially more compliant than the central ice stream. This figure also shows the two contours in margin size-compliance ratio space that would be sufficient to match the values of L_{tr} found for compliant margins models approximating observations of the semidiurnal and fortnightly tidal displacements at Rutford Ice Streams. In these cases, the minimum values of D are found to be: 0.988 for the fortnightly Rutford tide and 0.996 for the semidiurnal Rutford tide. However, as the shear margins for Rutford Ice Stream are on the order of 10 % full-width (e.g., Joughin et al., 2006), the values of D necessary to match L_{tr} would be even nearer to 1.0.

To add some physical meaning to these estimates of D , we compare these modeled values to the critical damage threshold values of D , commonly named D_C , found in the literature. D_C is the linear damage value at which a material becomes sufficiently fractured to stop behaving as a single continuous body. From laboratory experiments, D_C has been approximated from between 0.45–0.56 for ice (Pralong and Funk, 2005; Duddu and Waisman, 2012). From analysis and numerical inverse modeling of a continuum damage mechanical viscous model of the Larsen B Ice Shelf collapse, Borstad et al. (2012) found the value of D_C for calving to be 0.6 ± 0.1 . To compare D_C with our model results, we must remember that the above values for D_C are for nonlinear viscous flow, such that the “enhancement” value is governed by:

$$En = (1 - D)^{-n} \quad (8)$$

Modeling the elastic transmission of tidal stresses to great distances

J. Thompson et al.

Title Page

Abstract

Introduction

Conclusions

References

Tables

Figures

⏪

⏩

◀

▶

Back

Close

Full Screen / Esc

Printer-friendly Version

Interactive Discussion



Thus, the corresponding enhancements are between about 6 (for 0.45) and 37 (for 0.7) using the canonical power law exponent for Glen flow of $n = 3$. Even the smallest necessary enhancement has a value of 467.7 ($10^{2.67}$, for the fortnightly tide on Rutford Ice Stream), suggesting that the damage required to have sufficient marginal compliance to match the values of L_{tr} is too high to be physically reasonable. Thus, we find that a damage-based marginal compliance model is insufficient to bring model-predicted estimates of L_{tr} into line with those found observationally from GPS stations on Rutford Ice Stream.

5 Viscoelasticity

We now investigate the potential for viscoelasticity to decouple the ice stream from its lateral margins and thus increase the transmission length-scale of a tidal load. As an ice stream's margin is the location of large shear stresses, a stress-dependent viscoelasticity will necessarily have reduced viscosity in the ice stream margins. The net result would be the decoupling of the ice stream from its margins by concentrating deformation near the margins, allowing for a longer transmission of a tidal stress perturbation.

Incorporating both viscoelasticity and nonlinearity into the constitutive law for ice introduces many additional modeling concerns in order to correctly describe the link between ocean tides and ice stream motion. A model with stress-dependent viscosity should not neglect background flow stresses within the ice stream. In our models, we apply the downhill (i.e., deviatoric) portion of the gravitational driving stress. In the finite element formulation, we apply the horizontal component of gravity, with a magnitude of $g_{horiz} = g \sin \alpha$, as a time-constant acceleration acting on the entire ice body. We then apply the tidal loading as in our linear elastic models; see Appendix B for a discussion the tidal loading condition in the context of our viscoelastic models.

As viscous deformation is a time-dependent process, these viscoelastic models must explicitly account for the time-variability of a tidal loading condition. We use three main

Modeling the elastic transmission of tidal stresses to great distances

J. Thompson et al.

Title Page

Abstract

Introduction

Conclusions

References

Tables

Figures



Back

Close

Full Screen / Esc

Printer-friendly Version

Interactive Discussion



Modeling the elastic transmission of tidal stresses to great distances

J. Thompson et al.

Title Page

Abstract

Introduction

Conclusions

References

Tables

Figures

⏪

⏩

◀

▶

Back

Close

Full Screen / Esc

Printer-friendly Version

Interactive Discussion

tidal constituents (i.e., the semidiurnal, diurnal, and fortnightly tides) as forcing functions in our nonlinear viscoelastic finite element models. For simplicity, we approximate the tidal periods of these tidal constituents as 12 h, 24 h, and 14 days, respectively. As a reminder, the three tidal constituents cannot strictly be separated due to the nonlinearity of the viscous deformation, and research by Gundmundsson (2006, 2007, 2011) suggests that fortnightly variability in ice stream motion is a consequence of the nonlinear interaction of the semidiurnal ocean tides. However, modeling the response of an ice stream model to a single tidal component is more straightforward and provides an estimate of the expected change in stress-transmission as a function of the tidal forcing period. To ensure that the model is appropriately “spun-up” (e.g., Hetland and Hager, 2005), we only present results that have been run long enough such that the detrended, oscillatory motion is consistent over consecutive tidal cycles.

A final consideration is the strong temperature dependence of the ice viscosity (e.g., Weertman, 1983; Hooke and Hanson, 1986; Paterson, 1994; Cuffey and Paterson, 2011). The temperature dependence of the viscosity coefficient, from Cuffey and Paterson (2011), is:

$$A = 3.5 \times 10^{-25} \exp \left(\frac{-6 \times 10^4}{8.314} \cdot \left[\frac{1}{T} - \frac{1}{263} \right] \right) \text{ Pa}^{-3} \text{ s}^{-1} \quad \text{for } T < 263 \text{ K} \quad (9)$$

$$A = 3.5 \times 10^{-25} \exp \left(\frac{-1.39 \times 10^5}{8.314} \cdot \left[\frac{1}{T} - \frac{1}{263} \right] \right) \text{ Pa}^{-3} \text{ s}^{-1} \quad \text{for } T > 263 \text{ K}$$

where T is measured in degrees Kelvin. Antarctic ice streams have been observed to have a strong temperature gradient from base to surface (e.g., Engelhardt et al., 1990; Engelhardt and Kamb, 1993, 1998; Engelhardt, 2004a, b), with some ice stream beds up to 20 K warmer than the ice stream’s surface. We adopt an empirical fit of temperature data from Whillans Ice Stream as the temperature profile in all models. The temperature gradient of such a temperature profile is defined by Engelhardt and

Kamb (1993) as:

$$\frac{dT}{dz} = q_b e^{-y^2} + \frac{\lambda a u l}{\kappa} e^{-y^2} \int_0^y e^{-t^2} dt \quad (10)$$

where $y = z/l$, $l = 2\kappa H/a$, q_b is the basal temperature gradient, a is the accumulation rate, u is the ice stream horizontal velocity, κ is the thermal diffusivity, H is the ice stream thickness, and λ is the temperature gradient in air. All values of these parameters, save for model geometries, are taken from Engelhardt and Kamb (1993). In solving for the temperature profile, we set the basal temperature equal to the pressure melting point of ice, -0.7°C .

Our primary interest in modeling viscoelasticity is to determine if stress-dependence of viscosity results in a substantial decoupling of the ice stream from its lateral margins due to the higher stress concentration along the lateral margins. Recalling our earlier comparisons to the estimated tidal stress decay over Rutford Ice Stream, viscoelasticity would need to increase the value of L_{tr} by between a factor of two to four to match the field observations of Gudmundsson (2007, 2008, 2011). In order to find the correct amplitude and phase, we fit stress profiles along the modeled ice stream's length with:

$$\sigma_{yy} = A \sin(\omega t + \varphi) \quad (11)$$

where A is the stress amplitude, ω is the tidal frequency of the applied tide, and φ is the phase delay. We then can use the distance dependence of A to calculate a value of L_{tr} because in all these oscillatory models, we observe an exponential decay of amplitude with distance inland of the grounding line.

Figure 10 shows the values of L_{tr} , stress, and phase delay for a representative model using a semidiurnal tide. The modeled stress transmission length-scales for these viscoelastic models are summarized in Table 6. From this table, we see that incorporating a temperature-dependent viscosity increases L_{tr} by less than 50% for all tidal frequencies – insufficient to match the observations.

Modeling the elastic transmission of tidal stresses to great distances

J. Thompson et al.

Title Page

Abstract

Introduction

Conclusions

References

Tables

Figures

⏪

⏩

◀

▶

Back

Close

Full Screen / Esc

Printer-friendly Version

Interactive Discussion



Modeling the elastic transmission of tidal stresses to great distances

J. Thompson et al.

Title Page

Abstract

Introduction

Conclusions

References

Tables

Figures

⏪

⏩

◀

▶

Back

Close

Full Screen / Esc

Printer-friendly Version

Interactive Discussion

that an axially forced block, when restrained from below, has a stress field that is only important local to the edge of the applied load. Additionally, Goodier establishes the same conclusion when the block is fixed from both above and below. These two cases are identical to our 2-D model with a fixed base and the 2-D version (in map view) of our 3-D ice stream model, respectively. Timoshenko and Goodier (1982) provide an explicit form of the stress solution for similar, albeit not identical, models. In their article 24, they describe the expectation of exponential decay of stress with distance away from a point load applied to the opposite edges of a beam. Thus, it should not be a surprise that we find an exponential decay of stresses in these ice stream models.

As mentioned in the introductory section, previous models for the transmission of tidal stresses in ice streams suggest that there is an exponential decay of stress with distance inland of the grounding line (e.g., Anandakrishnan and Alley, 1997; Sergienko et al., 2009). We first compare our results to those of Anandakrishnan and Alley (1997); our 2-D model results represent extremes of Anandakrishnan and Alley's model. The frozen bed model corresponds to Anandakrishnan's and Alley's model with either a zero-thickness viscous layer or an infinitely viscous ($\eta \approx \infty$) layer. The sliding bed model corresponds to Anandakrishnan and Alley's model with an infinitely weak ($\eta \approx 0$) viscous layer. As the two-layer models of Anandakrishnan and Alley have the additional free parameter of till viscosity, these models can either constrain the viscosity of the viscous till layer using the transmission length of stress, or constrain the transmission length of stress using the till viscosity, but not both simultaneously. Additionally, the lack of lateral restraint in the model allows for the physically unrealistic case of infinite stress-transmission. The same issue is present in all the flow-line models, and as such, the two-dimensional assumption of negligible lateral resistance is not physically realistic for channelized ice streams.

Of the published models considered earlier, Sergienko et al. (2009) is the only study to explicitly account for lateral resistances. Removing the basal drag condition from Sergienko et al.'s model results in a 1-D approximation of our 3-D modeling. However, the lack of a length-scale relationship for the elastic springs in Sergienko et al.'s model

Modeling the elastic transmission of tidal stresses to great distances

J. Thompson et al.

Title Page

Abstract

Introduction

Conclusions

References

Tables

Figures

⏪

⏩

◀

▶

Back

Close

Full Screen / Esc

Printer-friendly Version

Interactive Discussion

prevents us from directly applying this model to constrain a stress-transmission length-scale. As our finite element modeling shows, the presence of non-sliding lateral margins and a zero-sliding basal condition both result in exponential decay of a tidal load with distance inland of the grounding line. Thus over the stick-slip cycle in Sergienko et al.'s paper, we expect that the stress-transmission would cycle between a thickness-controlled value when stuck and a width-controlled value when slipping.

In our 3-D models, ice stream width is the primary geometric control on L_{tr} , with ice stream thickness having only a minor role (~ 5 – 10% change per kilometer of thickness). Extending these results, models with a realistic geometry will only vary substantially from the equivalent box model approximation if the real ice stream's width changes dramatically along the flow direction. The width of Rutford Ice Stream does not change significantly through the region with CGPS observations.

We have shown that introducing variability in the elastic moduli can have a pronounced effect on L_{tr} . However, the precise change in L_{tr} depends on the choice a damage parameter and the shear margin size. Generally, increasing the damage (and thus elastic compliance) in the ice stream margins increases the value of L_{tr} . If we want to model marginal damage that will increase L_{tr} to a value large enough to match observations, we must choose a damage coefficient significantly higher than that proposed for calving in the ice shelf ($D \sim 0.99 > 0.6 \pm 0.1$). The ice stream is almost certainly not more damaged than its calving ice shelf, as otherwise having a cohesive ice shelf would be impossible.

Similarly, the viscoelastic models presented here demonstrate that the reduction in model viscosity due to the flow-induced shear is insufficient to dramatically perturb the state of stress within an ice stream. While L_{tr} increases slightly for models with temperature-dependent viscosity, such an increase falls far below that necessary to rectify the model results with the observations from Rutford Ice Stream, for all three tidal frequencies investigated here. For comparison, the change in L_{tr} from viscoelasticity is comparable to the change in L_{tr} due to increasing compliance in the lateral margins for physically realistic damage parameters.

6.1 Rutford ice stream

We now compare the observed decay of GPS surface displacements from Rutford Ice Stream to our modeled decay of stresses predicted using a geometry approximating Rutford Ice Stream. Recall that for linear elasticity, an exponential decay of stress will necessarily predict an exponential decay of displacement with the same decay rate, so such a comparison is strictly true for linear elastic models, and is approximate for viscoelastic models. The estimated L_{tr} for geometries approximating Rutford Ice Streams is 38.2 km (flagged model in Table 4). We note that our geometrically-simple model assumes that both margins are equally strong; in actuality, Rutford Ice Stream has one ice–ice interface and one ice–rock interface. However, based on the velocity profile for Rutford Ice Stream (Joughin et al., 2006), the difference between Rutford’s lateral margins does not appear to strongly control the behavior of the ice stream as a whole, allowing us to make a first-order approximation of Rutford as having strong, non-frictional boundary conditions on both lateral margins.

Figure 7b demonstrates that the decay is too severe to match the maximum observed displacement at stations inland of the grounding line (GPS data reported Gudmundsson, 2007 and was provided by H. Gudmundsson). This figure shows that the mechanisms of extreme-but-physically-reasonable damage, viscoelasticity, and both mechanisms combined linearly cannot modify the modeled values of L_{tr} to match the observed tidal deformation magnitudes. The implicit assumption in our models – that stress is transmitted through the bulk of the ice stream either elastically or viscoelastically – is not consistent with the observations from Rutford Ice Stream.

In the 2-D model of Gudmundsson (2011, “RIS flow-line model”), the surface velocity perturbations on Rutford Ice Stream due to the ocean tides are reproduced to good approximation when both a basal sliding law and ice viscoelasticity control the propagation of the tidal load inland of the grounding line. The results presented in this paper differ from those of the RIS flow-line model due to the following modeling differences:

Modeling the elastic transmission of tidal stresses to great distances

J. Thompson et al.

Title Page

Abstract

Introduction

Conclusions

References

Tables

Figures



Back

Close

Full Screen / Esc

Printer-friendly Version

Interactive Discussion

Modeling the elastic transmission of tidal stresses to great distances

J. Thompson et al.

Title Page

Abstract

Introduction

Conclusions

References

Tables

Figures

◀

▶

◀

▶

Back

Close

Full Screen / Esc

Printer-friendly Version

Interactive Discussion

1. Gudmundsson (2007) justifies the implicit neglect of the lateral margins in the RIS flow-line model by approximating the inland stress transmission of a tidal load as being at least four times the ice stream width, based on a stress transmission relationship developed for the vertical communication of stress through an ice stream in Gudmundsson (2003). Our modeling find that the lateral margins of the ice stream induce an exponential decay of a tidal load, and that a tidal stress falls by an order of magnitude over a distance of between 1.2 and 1.5 times the ice stream width.
2. In the models presented here, the ice stream width is the primary control on the value of L_{tr} , while in the RIS flow-line model, the basal resistance, ice thickness, and ice rheology are the controlling factors in the inland transmission of a tidal stress. As discussed above, we find that even in a frictionless model, the ice stream's width is a stronger control on the stress state of an ice stream than the ice thickness and ice rheology.
3. Gudmundsson (2011) implies that the flexural stress of the tides is the flow-controlling tidal stress. In all of our 2-D models, flexural stress decays within a few ice thicknesses of the grounding line – a result that matches observations of ice flexure (Stephenson, 1984; Rignot, 1998; Heinert and Riedel, 2007; Brunt et al., 2010).
4. Our modeling attempts to decouple the modeled ice stream from its lateral margins using shear-weakened ice and/or viscoelasticity were unable to rectify the model with the RIS flow-line model. To match the RIS flow-line model, our model would need to be decoupled from its lateral margins to such an extent that the model would exhibit deformation only along the extreme margins of the ice stream (i.e., “plug-like” deformation). InSAR surface velocities of Rutford Ice Stream (Joughin et al., 2006) do not show this “plug-like” pattern, suggesting strongly that such large-scale decoupling is not occurring.

6.2 Other ice stream geometries

Generally, the models presented here demonstrates that channelized ice streams, even under the favorable conditions of frictionless beds, enhanced marginal shear, and viscoelastic flow, fail to reproduce the length-scale of stress transmission observed in nature. Therefore, the models presented here draw into question the hypothesis that the observed influence of ocean tides on ice stream motion is universally an elastic process. However, we only consider a very specific range of ice stream geometries here: ice streams that have relatively narrow widths and strong ice–ice interfaces on the lateral margins. Two other Antarctic ice streams have observations of tidally-modulated surface displacements (Bindschadler and Whillans Ice Streams). For these ice streams, the assumption of ice–ice interfaces is appropriate but using channelized ice stream geometry is a poor approximation, as these ice streams have nearly equal widths and lengths near the grounding line. Broadly, our results are sufficient to demonstrate that a wider ice stream should have a larger stress transmission length-scale than a narrower ice stream. Nevertheless, the underlying geometric constrains on an ice stream impose exponential stress decay even for wide ice streams. Thus, these results may also approximately describe the stress behavior of wide ice streams in addition to channelized ice streams. However, the use of more appropriate ice stream geometries for ice streams with a similar width and length is beyond the scope of this paper.

6.3 An alternative mechanism for the transmission of tidal stresses

We conclude that for channelized ice streams, a process external to the ice stream is required for the impact of ocean tidal loads to extend far inland of the grounding line. While not explored in great detail here, our preferred hypothesis is that the ocean tides perturb the nature of streaming through the subglacial hydrologic network. Since the basal traction beneath these fast-moving ice streams must be small in order to encourage sliding and since these Antarctic ice streams are underlain by water-logged

Modeling the elastic transmission of tidal stresses to great distances

J. Thompson et al.

Title Page

Abstract

Introduction

Conclusions

References

Tables

Figures

⏪

⏩

◀

▶

Back

Close

Full Screen / Esc

Printer-friendly Version

Interactive Discussion



Modeling the elastic transmission of tidal stresses to great distances

J. Thompson et al.

Title Page

Abstract

Introduction

Conclusions

References

Tables

Figures

◀

▶

◀

▶

Back

Close

Full Screen / Esc

Printer-friendly Version

Interactive Discussion

tills (e.g., Alley et al., 1986; Smith, 1997; Engelhardt and Kamb, 1998; Tulaczyk et al., 2000a; Adalgeirsdottir et al., 2008; Raymond Pralong and Gudmundsson, 2011), the fluid pressure within the subglacial till is likely sufficient to cause the till to deform plastically, or at least highly nonlinearly. Our hypothesis is that the change in ocean tidal height, coupled with the tidal migration of till pore pressures, can move the onset of highly weakened till inland and seaward over the course of a tidal cycle. As demonstrated by Fig. 12, when the onset of till weakening is pushed inland, the ice stream at a given point should increase velocity as a longer portion of the glacier is unresisted basally. The opposite is true when the onset of till weakening moves towards the ocean. Furthermore, as the magnitude of the fluid pressure perturbation due to the ocean tide should decay with distance inland of the grounding line, the effect is expected to be most pronounced near the grounding line.

To derive an analytical form for this conceptual model, we start by following the 2-D, flow-line approach of Gudmundsson (2007), and assume that the basal velocity of the ice stream is a nonlinear function of the basal stress:

$$u_b = A\tau_b^\eta \quad (12)$$

where A is a rheological coefficient, and $\eta \neq 1$. We now assume that τ_b is also modulated by an effective shear stress, $\sigma_e = \sigma_0 - p$ (where p is the local fluid pressure) through a Coulomb-type rheology, the expected model for Antarctic till (e.g., Tulaczyk, 2000). If the connectivity of the till is high (i.e., infinitely fast), then the fluid pressure is:

$$p(x, t) = p_0 + \rho gh(t) \quad (13)$$

where $h(t)$ is the tidal height at the grounding line. If instead the connectivity is low enough that there is a resistance to flow, then one might expect the fluid pressure to instead be:

$$p(x, t) = p_0 + \rho gh(t - x/U) \quad (14)$$

where U is the flow velocity for a turbulent flow through (a channelized) subglacial till (after Manning, 1891; Tsai and Rice, 2010):

$$U = \frac{1}{0.038 \times k^{1/6}} R^{2/3} \left(\frac{dh}{dx} \right)^{1/2} \quad (15)$$

where k is the Nikuradse roughness height for the till and R is the radius of the flow channel. In either case, for till rheology, the basal stress is:

$$\tau_b = f \sigma_e = \tau_{b0} - f \rho g h (t - x/U) \quad (16)$$

where f is the friction angle, which is typically $f \leq 0.6$. If we define the basal velocity u_b by Eq. (12), then the current model's form, with infinitely high connectivity, is exactly equivalent to the model of Gudmundsson (2007) except that Gudmundsson's constant K is replaced with f . In particular, this conceptual model achieves the same large fortnightly variability in velocities with forcing only at semidiurnal periods M_2 and S_2 . Furthermore, for the case of finite connectivity, the turbulent flow velocity U takes the place of the viscoelastic relaxation speed of Gudmundsson (2011). We have essentially replaced the elastic and viscoelastic material parameters of Gudmundsson (2007, 2011) with till material and fluid flow parameters. If we take reasonable values of $\frac{dh}{dx} = \frac{5\text{m}}{10^4\text{m}} = 0.0005$, $k = 0.1\text{m}$, and $R = 0.1\text{m}$, we find that $U \approx 0.2\text{m s}^{-1}$. Taking $f \approx 0.2$, the observations from Rutford Ice Stream can be explained using our hydraulic model as well as the viscoelastic model of Gudmundsson (2011), but without the problems of elastic stress transmission discussed in the earlier sections of this paper. A more precise evaluation of this hydraulic model, such as including the effect of the decay of fluid pressure perturbation upstream, is beyond the scope of this paper, but could provide method for constraining basal friction and hydrologic connectivity using the observed decay of tidal stresses on Antarctic Ice Streams.

Modeling the elastic transmission of tidal stresses to great distances

J. Thompson et al.

Title Page	
Abstract	Introduction
Conclusions	References
Tables	Figures
◀	▶
◀	▶
Back	Close
Full Screen / Esc	
Printer-friendly Version	
Interactive Discussion	



7 Conclusions

From our modeling, we find:

1. For models supported either at the bed or at the margins, an axially applied tidal load decays exponentially with distance inland of the grounding line. Furthermore, for a reasonable elastic or viscoelastic model, this decay is too severe to transmit stresses far enough inland to explain surface observations from several Antarctic ice streams.
2. The ice shelf and the resulting flexural stresses are relevant only local to the grounding line, and can be safely neglected for problems of stress transmission many tens of kilometers inland of the grounding line.
3. Having compliant lateral margins in an ice stream can increase the distance to which stresses transmit, but this occurs in a highly nonlinear fashion. Using a linear damage mechanics model, we find that we would need damage resulting in upwards of a 99.9% reduction in Young's modulus to rectify model results with observations.
4. A Glen-style viscoelastic rheology using canonical values and a realistic temperature profile does not change the transmission of stress in any meaningful fashion when the temperature dependence of ice is taken into account.

Our modeling demonstrate the importance of approaching the tidal loading on an ice stream as a three-dimensional problem due to the stress support provided by the lateral margins of the ice stream to a tidal load. We cannot find a reasonable set of elastic or viscoelastic parameters, homogenous or otherwise, that can reproduce the observations of tidal stresses from Rutford Ice Stream when we include the finite width of the ice stream in our models.

As we could not match observations using an elastic or viscoelastic model for the transmission of tidal stresses, we presented a 2-D, flow-line model for the transmission

Modeling the elastic transmission of tidal stresses to great distances

J. Thompson et al.

Title Page

Abstract

Introduction

Conclusions

References

Tables

Figures

⏪

⏩

◀

▶

Back

Close

Full Screen / Esc

Printer-friendly Version

Interactive Discussion



Modeling the elastic transmission of tidal stresses to great distances

J. Thompson et al.

Title Page

Abstract

Introduction

Conclusions

References

Tables

Figures

◀

▶

◀

▶

Back

Close

Full Screen / Esc

Printer-friendly Version

Interactive Discussion

of a tidal perturbation inland of the grounding line through the fluid pressure within subglacial till. Using reasonable material parameters, we demonstrated that this model can reproduce the modeling results of Gudmundsson (2011) for Rutford Ice Stream's tidally modulated motion, but without the need to rely on stress transmission through the bulk of the ice stream. Thus, we conclude that for channelized ice streams such as Rutford Ice Stream, and perhaps for other tidally-modulated ice streams as well, stress transmission through the subglacial hydrologic network is the most-likely mechanism for the tidal modulation of ice stream motion at great distances inland of the grounding line.

Appendix A

Importance of the ice shelf

As all of the ice streams that display far-field tidal effects have a connected ice shelf, we now consider the role that the ice shelf plays as the intermediary between the ocean tides and the grounded ice stream. Recall the two-dimensional model results shown in Figs. 3 and 4 for models both with and without an ice shelf. For a given basal condition, any variation between the two model results must be due to the presence of the shelf alone.

For the model with a frozen base, the presence of an ice shelf has two effects. First, there is a perturbation to the stress field near the grounding line (about two kilometers inland at most), due to flexural stresses introduced by the ice shelf. Second, the overall magnitude of stresses in the ice stream is elevated compared to models with only axial loading as there is an overall increase in the magnitude of the loading applied in the model. This effect does not change L_{tr} . Thus for ice with no basal sliding, including an ice shelf affects the magnitude, but not the nature of the stress field, far inland of the grounding line.

Modeling the elastic transmission of tidal stresses to great distances

J. Thompson et al.

Title Page

Abstract

Introduction

Conclusions

References

Tables

Figures

◀

▶

◀

▶

Back

Close

Full Screen / Esc

Printer-friendly Version

Interactive Discussion

For the two-dimensional model with basal sliding, stresses due to ice flexure decay to inconsequential levels 5–7 km inland of the grounding line. Beyond this point, the stress state of the ice stream is identical to the stress state for a model with axial loading only. Thus, for an ice stream with no basal resistance, the ice shelf does not influence the modeled results farther inland than less than the first ten kilometers of grounded ice.

The general results that flexural stresses only perturb the stress field near the grounding line is consistent with the observations of ice flexure transmission of ten kilometers or less, as summarized in Table 1. Additionally, the constant-loading shelf condition overestimates flexural stress by almost a factor of four compared to a more realistic floating condition (see Appendix C), meaning that flexural stresses may decay to small values over shorter distance than predicted here. These models reproduce the observation that the flexural stresses, as induced by the presence of an ice shelf, are not important far inland of the grounding line.

The basal condition beneath the ice stream determines the influence of the ice shelf on the overall magnitude of the stress in the far-field ice stream. As ice streams have little basal resistance, the result that the overall stress magnitude is independent of the ice shelf outside of the flexure zone is applicable as our interest is in the value of stresses at many tens of kilometers inland of the grounding line, we can safely neglect the ice shelf in these models without changing the transmission of tidal, non-flexural stresses.

Appendix B

Viscoelastic tidal loading

Following the rationale of Cuffey and Paterson (2011) (and references therein), the stress balance for an ice stream/shelf system would involve balancing the hydrostatic pressure at the edge of the ice shelf and that of the ocean. As the ice shelf is floating, there is a net “pull” on the ice stream due to the excess pressure in the ice shelf com-

Modeling the elastic transmission of tidal stresses to great distances

J. Thompson et al.

Title Page

Abstract

Introduction

Conclusions

References

Tables

Figures

⏪

⏩

◀

▶

Back

Close

Full Screen / Esc

Printer-friendly Version

Interactive Discussion

pared to that of the ocean. As ice viscosity is stress dependent, to be strictly accurate, we need to account for this end stress in our models to accurately model the viscous deformation in the ice stream. However, as the problem is more numerically tractable with a simple oscillatory tidal condition based on the elastic loading condition, we compare the model output for these two tidal loads (called “full” and “simple,” respectively). We find that having the more complex full tidal condition changes the length-scale for stress-transmission decay, L_{tr} , by only about 20 %, far below the factor of 3–4 change necessary to match observations. Thus, we use this as justification to use the more numerically favorable simple tidal condition.

B1 Full tidal loading condition

In addition to the oscillatory load of the ocean tide, there are three major tidally-important stresses that a full tidal loading condition needs to consider. These stresses are incorporated into the balance of: the hydrostatic pressure of the flowing ice, the hydrostatic pressure of the static ocean water, and the flexural stress imposed on the grounding line due to the vertical motion of the ice shelf. Figure B1 shows a schematic picture of the interaction of these stresses on an ice stream at neutral, high, and low tides.

First consider that the hydrostatic pressure of the ice and the water. For the ice, the value of the stress at a given depth is simply $\rho_I g(H_I - z)$. For the water, we first use the flotation condition at the grounding line to find that the water rises to a height of $H_T = H_I(1 - \rho_I/\rho_W)$, which in turn leads to the definition of the hydrostatic pressure at levels where water exists as: $\rho_W g(H_T - z)$. However, this stress balance occurs at the edge of the ice shelf, not at the grounding line. We make use of the assumption that the ice shelf behaves elastically, which, following the results from our 2-D shelf models in Sect. 4, allows us to move this stress balance to the grounding line without any decay of these stress values.

To account for the bending stress from ice flexure, we use the same simple beam theory presented in Appendix C. From this simple model for flexure, we expect that the

flexural stress at the grounding line will be on the order of a few 100 kPa at a maximum (the exact value depends on the ice thickness and the geometry of the ice shelf).

The full load applied at the grounding line is the sum of these three stresses: the differential gravitational stress at the end of the ice stream, the flexural stress induced by the floating ice shelf, and the change in water weight due to the tide. Figure B1 shows a graphical representation of these tidal loads, while Eq. (B1) shows the total form of this loading:

$$\sigma_{\text{applied}} = \begin{cases} -\rho_I g(H_I - z) & \text{if } z > H_T \\ -\rho_I g(H_I - z) + \rho_W g(H_T - z) & \text{if } z \leq H_T \end{cases} \quad (\text{B1})$$

$$+ F_{\text{Tide}}(t) \times \left[\sigma_{\text{flex}} \Delta h \left(z - \frac{1}{2} H_I \right) + \rho_W g \Delta h \right] \quad (\text{B2})$$

where H_I is the ice thickness, H_T is the water level relative to the base of the ice stream, $F_{\text{Tide}}(t)$ is a unit tidal forcing as a function of time, and σ_{flex} is the maximum amplitude of flexure for a unit tide. For a reasonable tidal loading, the maximum force comes from the static “pull”, which is on the order of 1 MPa at the base of a one-kilometer-thick ice stream, while the flexural stress is a few 100 kPas and the tidal weight is a few 10 kPas.

B2 Simple tidal loading condition

For the simple loading condition, we apply the variable portion of the ocean tidal load as a normal traction to the grounding line. Mathematically, this condition is:

$$\sigma_{\text{applied}} = F_{\text{Tide}}(t) + \rho_W g \Delta h \quad (\text{B3})$$

This is identical to the approach taken in our linear elastic models, except that the applied stress is time-variable.

B3 Stress transmission comparison

Figure B2 shows a comparison between the tidally induced σ_{yy} component of stress (as described in Sect. 3.3.1) for a map view of the base of a model with the full (left) and simple (right) loading conditions taken at a peak in stress response. We first note that overall, the stress field is remarkably similar between the full and simple loading conditions. The only major difference occurs in the portion of the ice stream near the grounding line, where the full loading condition has elevated stress values than those of the simple loading model. Such an increase in the value of the stress near the grounding line in the full model is not surprising as the value of the applied load is larger in this model than with the simple loading condition.

However, beyond this point inland, the model stress states are nearly indistinguishable, suggesting strongly that neither the hydrostatic “pull” on the ice stream edge nor the flexural stress due to the ice shelf bending viscosity of the ice stream near the grounding line significantly enough to dramatically change the nature of the transmission of stress viscoelastically in the ice stream. Such results are keeping with the earlier observation and model results suggesting that tidal flexure is a stress that is only seen locally to the grounding line. The similarity in the model results is reflected in the values of L_{tr} calculated between these two models, which fall within 20% of one another.

As the difference between model results in this case is only on the order of 20%, we feel safe in neglecting the full tidal loading condition for our purposes. In the current form of the problem, we are sensitive to changes in the value of L_{tr} that amount to a factor of 3–4, and thus 20% is far below the threshold of usefulness to justify the increase complexity (and thus computation time) of running these models with the full loading condition.

Modeling the elastic transmission of tidal stresses to great distances

J. Thompson et al.

Title Page

Abstract

Introduction

Conclusions

References

Tables

Figures

⏪

⏩

◀

▶

Back

Close

Full Screen / Esc

Printer-friendly Version

Interactive Discussion

Appendix C

Analysis of the flotation condition for a one-dimensional ice shelf

As shown in Fig. 2, we apply two tractions to a model ice shelf to simulate the stress change on an ice shelf due to a change in tide height. First, we consider the axial load of the tide on the ice shelf's edge. A simple comparison is to look at the stress within an axial bar that is compressed axially with a constant stress. Take the bar to be fixed at the unforced end. By the compatibility condition:

$$\delta\sigma/\delta x = 0 \quad (\text{C1})$$

the stress and strain in such a model must be constant throughout the bar. This corresponds to infinite stress transmission.

Second, we model the ice shelf as a Bernoulli-Euler beam subjected to a distributed load, with this load coupled to the beam deflection by a flotation condition. This approach is similar to the methodology of Reeh et al. (2000). The governing equation of such a model is:

$$EI \frac{\delta^4 w}{\delta x^4} = \rho_w g (\Delta h - w) \quad (\text{C2})$$

where ρ_w is the density of water, g is gravitational acceleration, w is the (vertical) deflection of the beam, E is the Young's modulus of ice, $I = \left(\frac{w}{12}\right) \cdot (h)^3$ is the second moment of area for the ice shelf.

The solution of this equation for multiple ice shelf lengths are found and shown in Fig. C1. The primary result is that, for a one meter tide, a shelf of longer than five kilometers no longer influences the stresses at the grounding line, meaning that for our purposes, we only need to consider a shelf of five kilometers length in our finite element modeling.

Additionally, we model a linearly thinning ice shelf (through the modification of I , using $I = \left(\frac{w}{12}\right) \cdot ([h_0 - (h_0 - h_1)] \frac{x}{L})^3$ where the thickness linearly changes from h_0 to h_1)

and find that this only has a small influence on the stress and deflection throughout the shelf. Thus these effects will not be considered further.

Lastly, we model the results for a simpler, uncoupled stressing condition. In Fig. C1, the red dashed line corresponds to a constant loading function equal to $\rho_W g \Delta h$. This simpler condition overestimates the stress and deflection over the model domain compared to the more correct flotation condition. However, as the boundary condition does not depend on, and thus is decoupled from, the deflection w , we use this constant loading as the ice shelf boundary “pseudo-flotation” condition in our finite modeling.

References

- 10 Aagaard, B. T., Knepley, M. G., and Williams, C. A.: A domain decomposition approach to implementing fault slip in finite-element models of quasi-static and dynamic crustal deformation, *J. Geophys. Res.-Sol. Ea.*, 118, 3059–3079, doi:10.1002/jgrb.502173059-3079, 2013a.
- Aagaard, B., Kientz, S., Knepley, M., Strand, L., and Williams, C.: PyLith User Manual, Version 1.9.0, Davis, CA: Computational Infrastructure of Geodynamics, available at: http://geodynamics.org/cig/software/pylith/pylith_manual-1.9.0.pdf (last access: 21 April 2014), 2013.
- 15 Anandakrishnan, S. and Alley, R. B.: Tidal forcing of basal seismicity of ice stream C, West Antarctica, observed far inland, *J. Geophys. Res.*, 102, 183–196, 1997.
- Anadakrishnan, S., Voigt, D. E., Alley, R. B., and King, M. A.: Ice stream D flow speed is strongly modulated by the tide beneath the Ross Ice Shelf, *Geophys. Res. Lett.*, 30, 1361, doi:10.1029/2002GL016329, 2003.
- 20 Balay, S., Gropp, W. D., McInnes, L. C., and Smith, B. F.: Efficient management of parallelism in object oriented numerical software libraries, in: *Modern Software Tools in Scientific Computing*, edited by: Arge, E., Bruaset, A. M., and Langtangen, H. P., Birkhauser Press, Boston, MA, 163–202, 1997.
- 25 Balay, S., Brown, J., Buschelman, K., Gropp, W. D., Kaushik, D., Knepley, M. G., McInnes, L. C., Smith, B. F., and Zhang, H.: PETSc Webpage, available at: mcs.anl.gov/petsc (last access: 28 May 2013), 2012a.

Modeling the elastic transmission of tidal stresses to great distances

J. Thompson et al.

Title Page

Abstract

Introduction

Conclusions

References

Tables

Figures

⏪

⏩

◀

▶

Back

Close

Full Screen / Esc

Printer-friendly Version

Interactive Discussion

- Balay, S., Brown, J., Buschelman, K., Eijkhout, V., Gropp, W. D., Kaushik, D., Knepley, M. G., McInnes, L. C., Smith, B. F., and Zhang, H.: PETSc Users Manual, ANL-95/11 – Revision 3.3, Argonne National Laboratory, online manual, available at: <http://www.mcs.anl.gov/petsc/petsc-current/docs/manual.pdf> (last access: 28 May 2013), 2012b.
- 5 Bathe, K.-J.: Finite-Element Procedures, Prentice Hall, Upper Saddle River, NJ, 1037 pp., 1995.
- Blankenship, D. D. and Bentley, C. R.: The crystalline fabric of polar ice sheets inferred from seismic anisotropy, *Int. Assoc. Hydrol. Sci.*, 170, 17–28, 1987.
- Borstad, C. P., Khazendar, A., Larour, E., Morlighem, M., Rignot, E., Schodlock, M. P.,
10 and Seroussi, H.: A damage mechanics assessment of the Larsen B ice shelf prior to collapse: towards a physically-based calving law, *Geophys. Res. Lett.*, 39, L18502, doi:10.1029/2012GL053317, 2012.
- Bindschadler, R. A., Vornberger, P. L., King, M. A., and Padman, L.: Tidally driven stick-slip motion in the mouth of Whillans Ice Stream, Antarctica, *Ann. Glaciol.*, 36, 263–272, 2003.
- 15 Brunt, K. M., Fricker, H. A., Padman, L., Scambos, T. A., and O’Neel, S.: Mapping the grounding zone of the Ross Ice Shelf, Antarctica, using ICESat laser altimetry, *Ann. Glaciol.*, 51, 71–79, 2010.
- Cuffey, K. M. and Paterson, W. S. B.: *The Physics of Glaciers*, 4th edn., Elsevier, San Diego, CA, 693 pp., 2010.
- 20 Dahl-Jensen, D. and Gundestrup, N. S.: Constitutive properties of ice at Dye 3, Greenland, *Int. Assoc. Hydrol. Sci.*, 170, 31–43, 1987.
- Echelmeyer, K. and Zhongxiang, W.: Direct observations of basal sliding and deformation of basal drift at sub-freezing temperatures, *J. Glaciol.*, 33, 83–98, 1987.
- Echelmeyer, K. A., Harrison, W. D., Larson, C., and Mitchell, J. E.: The role of the margins in the dynamics of an active ice stream, *J. Glaciol.*, 40, 527–538, 1994.
- 25 Engelhardt, H. and Kamb, W. B.: Basal sliding of Ice Stream B, West Antarctica, *J. Glaciol.*, 44, 223–230, 1998.
- Gammon, P. H., Kieffe, H., and Clouter, M. J.: Elastic-constants of ice samples by Brillouin spectroscopy, *J. Phys. Chem.*, 87, 4025–4029, doi:10.1021/j100244a004, 1983a.
- 30 Gammon, P. H., Kieffe, H., Clouter, M. J., and Denner, W. W.: Elastic-constants of artificial and natural ice samples by Brillouin Spectroscopy, *J. Glaciol.*, 29, 433–460, 1983b.
- Goodier, J. N.: An extension of Saint-Venant’s Principle, with applications, *J. Appl. Phys.*, 13, 167–171, 1942.

Modeling the elastic transmission of tidal stresses to great distances

J. Thompson et al.

Title Page

Abstract

Introduction

Conclusions

References

Tables

Figures

◀

▶

◀

▶

Back

Close

Full Screen / Esc

Printer-friendly Version

Interactive Discussion

- Gudmundsson, G. H.: Fortnightly variations in the flow velocity of Rutford Ice Stream, West Antarctica, *Nature*, 444, 1063–1064, doi:10.1038/nature05430, 2006.
- Gudmundsson, G. H.: Tides and the flow of Rutford Ice Stream, West Antarctica, *J. Geophys. Res.*, 112, F04007, doi:10.1029/2006JF000731, 2007.
- 5 Gudmundsson, G. H.: Ice-stream response to ocean tides and the form of the basal sliding law, *The Cryosphere*, 5, 259–270, doi:10.5194/tc-5-259-2011, 2011.
- Harrison, W. D., Echelmeyer, K. A., and Engelhardt, H.: Short-period observations of speed, strain and seismicity on Ice Stream B, Antarctica, *J. Glaciol.*, 39, 463–470, 1993.
- Heinert, M. and Riedel, B.: Parametric modelling of the geometrical ice–ocean interaction in the Ekstroemisen grounding zone based on short time-series, *Geophys. J. Int.*, 169, 407–420, doi:10.1111/j.1365-246X.2007.03364.x, 2007.
- 10 Hetland, E. A. and Hager, B. H.: Postseismic and interseismic displacements near a strike-slip fault: a two-dimensional theory for general linear viscoelastic rheologies, *J. Geophys. Res.*, 110, B10401, doi:10.1029/2005JB003689, 2005.
- 15 Hughes, T. J.: *Ice Sheets*, Oxford University Press, New York, NY, 343 pp., 1998.
- Jellinek, H. H. G. and Brill, R.: Viscoelastic properties of ice, *J. Appl. Phys.*, 27, 1198–1209, 1956.
- Joughin, I., MacAyeal, D. R., and Tulaczyk, S.: Basal shear stress of the Ross ice streams from control method inversions, *J. Geophys. Res.*, 109, B09405, doi:10.1029/2003JB002960, 2004.
- 20 Joughin, I., Bamber, J. L., Scambos, T., Tulaczyk, S., Fahnestock, M., and MacAyeal, D. R.: Integrating satellite observations with modeling: basal shear stress of the Flicher-Ronne ice streams, Antarctica, *Phil. T. Roy. Soc. A*, 364, 1785–1814, doi:10.1098/rsta.2006.1799, 2006.
- 25 Manning, R.: On the flow of water in open channels and pipes, *Trans. Inst. Civil Eng.*, 20, 161–207, 1891.
- Murakami, S.: *Continuum Damage Mechanics: a Continuum Mechanics Approach to the Analysis of Damage and Fracture*, Springer Science+Business Media, London, 402 pp., 2012.
- Nanthikensan, S. and Sunder, S. S.: Anisotropic elasticity of polycrystalline ice I_h , *Cold Reg. Sci. Tech.*, 22, 149–169, 1994.
- 30 Paterson, W. S. B.: Why ice-age ice is sometimes soft, *Cold Reg. Sci. Tech.*, 20, 75–98, 1991.
- Paterson, W. S. B.: *The Physics of Glaciers*, 3rd edn., Pergamon, New York, NY, 480 pp., 1994.

Modeling the elastic transmission of tidal stresses to great distances

J. Thompson et al.

Title Page

Abstract

Introduction

Conclusions

References

Tables

Figures

◀

▶

◀

▶

Back

Close

Full Screen / Esc

Printer-friendly Version

Interactive Discussion



- Petrenko, V. F. and Whitford, R. W.: Physics of Ice, 2nd edn., Oxford University Press, Oxford, England, 2002.
- Reeh, N., Mayer, C., Olesen, O. B., Christensen, E. L., and Thomsen, H. H.: Tidal movement of Nioghalvfjærdjorden glacier, northeast Greenland: observations and modelling, *Ann. Glaciol.*, 31, 111–117, 2000.
- Riedel, B. and Heinert, M.: First results of GPS array observations in the grounding zone of Ekstroem Ice Shelf, in: Oerter, H., comp. Filcher-Ronne Ice Shelf Programme (FRISP), Report No. 12, Alfred Wegener Institute for Polar and Marine Research, Bremerhaven, 74–76, 1998.
- Riedel, B., Nixdorf, U., Heinert, M., Eckstaller, A., and Mayer, C.: The response of the Ekstromisen (Antarctica) grounding zone to tidal forcing, *Ann. Glaciol.*, 29, 239–242, 1999.
- Rignot, E. J.: Fast recession of a west Antarctic glacier, *Science*, 281, 549, doi:10.1126/science.281.5376.549, 1998.
- Rosier, S. H. R., Gudmundsson, G. H., and Green, J. A. M.: Insights into ice stream dynamics through modeling their response to tidal forcing, *The Cryosphere Discuss.*, 8, 659–689, doi:10.5194/tcd-8-659-2014, 2014.
- Scott, J. B. T., Gudmundsson, G. H., Smith, A. M., Bingham, R. G., Pritchard, H. D., and Vaughan, D. G.: Increased rate of acceleration on Pine Island Glacier strongly coupled to changes in gravitational driving stress, *The Cryosphere*, 3, 125–131, doi:10.5194/tc-3-125-2009, 2009.
- Sergienko, O. V., MacAyeal, D. R., and Bindschadler, R. A.: Stick-slip behavior of ice streams: modeling investigations, *Ann. Glaciol.*, 50, 87–94, 2009.
- Stephenson, S. N.: Glacier flexure and the position of grounding lines: measurements by tiltmeter on Rutford Ice Stream, Antarctica, *Ann. Glaciol.*, 5, 165–169, 1984.
- Timoshenko, S. P. and Goodier, J. N.: Theory of Elasticity, 3rd. edn., McGraw-Hill Book Company, San Fransisco, CA, 567 pp., 1982.
- Tsai, V. C. and Rice, J. R.: A model for turbulent hydraulic fracture and application to crack propagation at glacier beds, *J. Geophys. Res.*, 115, F03007, doi:10.1029/2009JF001474, 2010.
- Walker, R. T., Christianson, K., Parizek, B. P., Anandakrishnan, S., and Alley, R. B.: A viscoelastic flowline model applied to tidal forcing of Bindschadler Ice Stream, West Antarctica, *Earth Planet. Sc. Lett.*, 319–320, 128–132, 2012.

Modeling the elastic transmission of tidal stresses to great distances

J. Thompson et al.

[Title Page](#)

[Abstract](#) | [Introduction](#)

[Conclusions](#) | [References](#)

[Tables](#) | [Figures](#)

[⏪](#) | [⏩](#)

[◀](#) | [▶](#)

[Back](#) | [Close](#)

[Full Screen / Esc](#)

[Printer-friendly Version](#)

[Interactive Discussion](#)

Walter, J. I., Brodsky, E. E., Tulaczyk, W., Schwartz, S. Y., and Pettersson, R.: Transient slip events from near-field seismic and geodetic data on a glacier fault, Whillans Ice Plain, West Antarctica, *J. Geophys. Res.*, 116, F01021, doi:10.1029/2010JF001754, 2011.

Weertman, J.: On the sliding of glaciers, *J. Glaciol.*, 3, 33–38, 1957.

5 Weertman, J.: The theory of glacier sliding, *J. Glaciol.*, 5, 287–303, 1964.

Wiens, D. A., Anandakrishnan, S., Winberry, J. P., and King, M. A.: Simultaneous teleseismic and geodetic observations of the stick-slip motion of an Antarctic ice stream, *Nature*, 453, 770–775, doi:10.1038/nature06990, 2008.

10 Winberry, J. P., Anandakrishnan, S., Alley, R. B., Bindschadler, R. A., and King, M. A.: Basal mechanics of ice streams: insights from the stick-slip motion of Whillans Ice Stream, West Antarctica, *J. Geophys. Res.*, 114, F01016, doi:10.1029/2008JF001035, 2009.



Modeling the elastic transmission of tidal stresses to great distances

J. Thompson et al.

Table 1. Spatial extent of tidal stress transmission and ice flexure from selected ice streams across Antarctica. Superscript numbers denote the following references: ¹ Anandakrishnan et al. (2003); ² Brunt et al. (2010); ³ Heinert and Riedel (2007); ⁴ Anandakrishnan and Alley (1997); ⁵ Scott et al. (2009); ⁶ Rignot (1998); ⁷ Gudmundsson (2006); ⁸ Gudmundsson (2007); ⁹ Stephenson (1984); ¹⁰ Weins et al. (2008); ¹¹ Winberry et al. (2009); ¹² Walter et al. (2011); ¹³ Harrison et al. (1993).

Region	Tidal Stress Transmission		Ice Flexure	
	Extent (km)	Method	Extent (km)	Method
Bindschadler	80+	GPS ¹	~ 10	Altimetry ²
Ekstrom	< 3	GPS ³	~ 5	Tilt ³
Kamb	85+	Seismicity ⁴	~ 10	Altimetry ²
Pine Island	< 55	GPS ⁵	~ 5	SAR ⁶
Rutford	40+	GPS ^{7,8}	5+	Tilt ⁹
Whillans Ice Plain	~ 100	GPS and Seismicity ^{10,11,12}	~ 10	Altimetry ²
Whillans Ice Stream	~ 300	Seismicity ¹³	N/A	Altimetry ²

Title Page

Abstract

Introduction

Conclusions

References

Tables

Figures

◀

▶

◀

▶

Back

Close

Full Screen / Esc

Printer-friendly Version

Interactive Discussion

Modeling the elastic transmission of tidal stresses to great distances

J. Thompson et al.

Table 2. Elastic and viscous parameters used to define the ice properties in our finite element modeling. Values of elastic parameters except for density are taken from Petrenko and Whitford (2002) using data from Gammon et al. (1983a, b). Viscous parameters are taken from Cuffey and Paterson (2010). Temperature-dependent viscosity coefficients are not summarized here but can be found in Cuffey and Paterson (2010). Parameters marked with ⁽¹⁾ denote quantities that are derived from the other moduli and material properties. Parameters marked with ⁽²⁾ are fixed through all models.

Parameter	Symbol	Value
Young's modulus	E	9.33 GPa
Poisson's ratio ²	ν	0.325
Shear modulus ¹	G	3.52 GPa
Bulk modulus ¹	K	8.90 GPa
Density (at 0 °C) ²	ρ	917 kgm ⁻³
Viscosity coefficient (at 0 °C) ²	A	$5.86 \times 10^{-6} \text{ MPa}^{-3} \text{ s}^{-1}$
Stress exponent ²	n	3

[Title Page](#)
[Abstract](#)
[Introduction](#)
[Conclusions](#)
[References](#)
[Tables](#)
[Figures](#)
[⏪](#)
[⏩](#)
[◀](#)
[▶](#)
[Back](#)
[Close](#)
[Full Screen / Esc](#)
[Printer-friendly Version](#)
[Interactive Discussion](#)


Modeling the elastic transmission of tidal stresses to great distances

J. Thompson et al.

Title Page

Abstract

Introduction

Conclusions

References

Tables

Figures

◀

▶

◀

▶

Back

Close

Full Screen / Esc

Printer-friendly Version

Interactive Discussion

Table 4. L_{tr} for 2-D models with a zero-displacement basal condition. Note that L_{tr} values are linear with thickness and independent of Young's modulus.

Thickness (km)	Young's modulus (GPa)	L_{tr} (km)
1	0.933	2.53
2	0.933	5.07
3	0.933	7.60
1	9.33	2.53
2	9.33	5.07
3	9.33	7.60
1	93.3	2.53
2	93.3	5.07
3	93.3	7.60

Modeling the elastic transmission of tidal stresses to great distances

J. Thompson et al.

Table 5. L_{tr} for 3-D models with uniform Young's moduli. Like the 2-D models, L_{tr} is effectively independent of Young's modulus, but increases with increasing thickness and width of the ice stream. The model indicated with (*) is representative of Rutford Ice Stream.

Thickness (km)	Width (km)	Young's modulus (GPa)	L_{tr} (km)
1	10	0.933	12.2
1	10	9.33	12.7
1	10	93.3	12.7
2	10	9.33	13.6
3	10	9.33	15.0
1	14	9.33	17.5
2	14	9.33	18.4
3	14	9.33	19.6
1	20	9.33	24.6
2	20	9.33	25.6
3	20	9.33	26.7
2	30	9.33	38.2*
2	40	9.33	52.2
2	50	9.33	69.1

Title Page

Abstract

Introduction

Conclusions

References

Tables

Figures

◀

▶

◀

▶

Back

Close

Full Screen / Esc

Printer-friendly Version

Interactive Discussion

Modeling the elastic transmission of tidal stresses to great distances

J. Thompson et al.

Table 6. Summary of the transmission length-scale for a tidal force, in kilometers, for our viscoelastic models. The viscosity column refers to whether the viscosity model is homogenous (homog.) or temperature-dependent (temp.). We include the homogenous models only for completeness since we consider the temperature-dependent models to be more physically representative of a real-world ice stream. The applied force describes the nature of the tidal loading applied in the model, as is described in Appendix C.

Tide	Applied Force	Viscosity	L_{tr} (km)
Semidiurnal	Full	Temp.	14.4
Semidiurnal	Simple	Temp.	16.4
Semidiurnal	Simple	Homog.	33.0
Diurnal	Full	Temp.	13.1
Diurnal	Simple	Temp.	12.8
Diurnal	Simple	Homog.	29.2
Fortnightly	Simple	Temp.	17.7
Fortnightly	Simple	Homog.	44.4

Title Page

Abstract

Introduction

Conclusions

References

Tables

Figures

◀

▶

◀

▶

Back

Close

Full Screen / Esc

Printer-friendly Version

Interactive Discussion

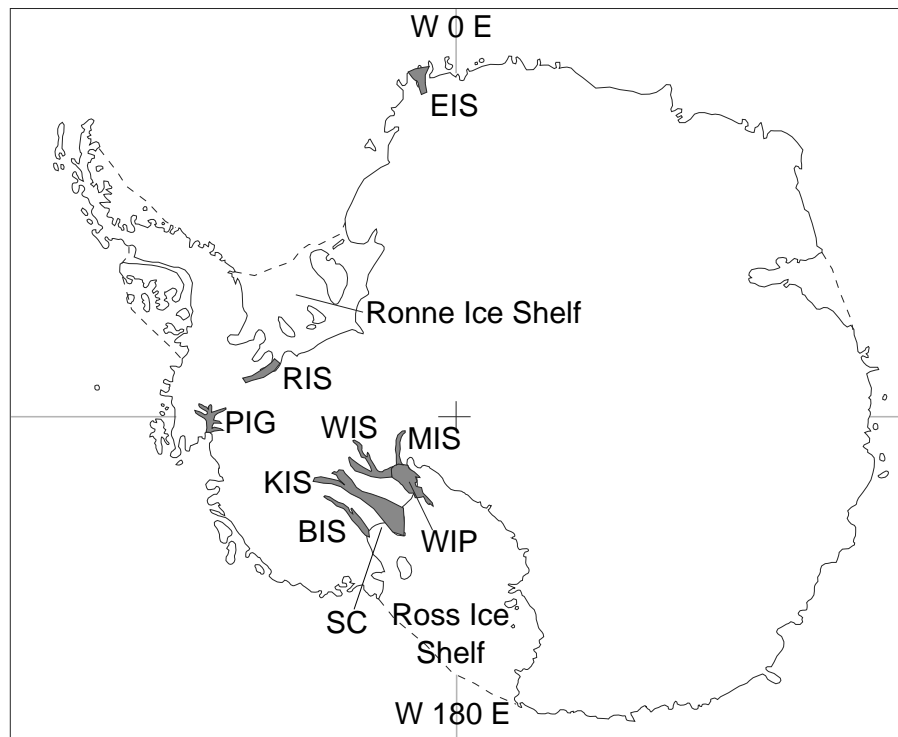


Fig. 1. Map of Antarctica indicating locations of the ice streams discussed in this paper (BIS-Bindschadler Ice Stream, EIS-Ekstrom Ice Stream, KIS-Kamb Ice Stream, PIG-Pine Island Glacier, RIS-Rutford Ice Stream, WIP-Whillans Ice Plain, WIS-Whillans Ice Stream, MIS-Mercer Ice Stream, SC-Siple Coast).

Modeling the elastic transmission of tidal stresses to great distances

J. Thompson et al.

Title Page	
Abstract	Introduction
Conclusions	References
Tables	Figures
◀	▶
◀	▶
Back	Close
Full Screen / Esc	
Printer-friendly Version	
Interactive Discussion	

Modeling the elastic transmission of tidal stresses to great distances

J. Thompson et al.

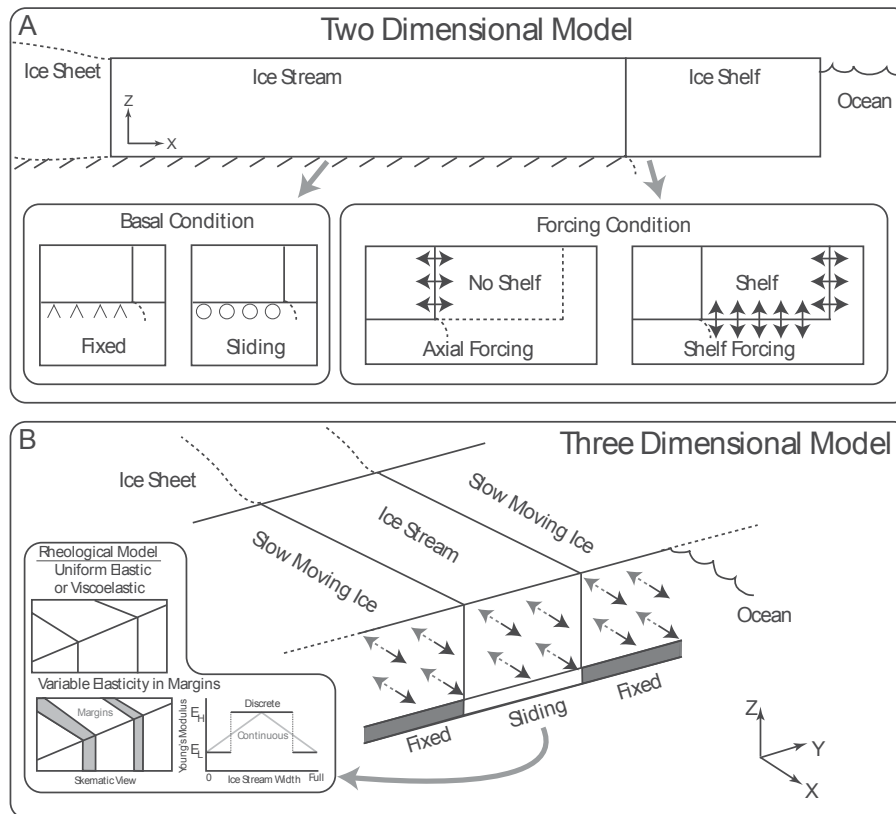


Fig. 2. Schematics of the models used in this paper. Inset boxes show options used in each model. For the two dimensional models, these are options are either a fixed ($u_x = u_z = 0$) or sliding ($u_z = 0$) basal condition, and either a pure axial loading condition or a shelf model. For the three dimensional models, we use the same model set up with either a uniform Young's modulus across the ice stream or marginal regions of weakened Young's modulus.

2D Model with Basal Sliding

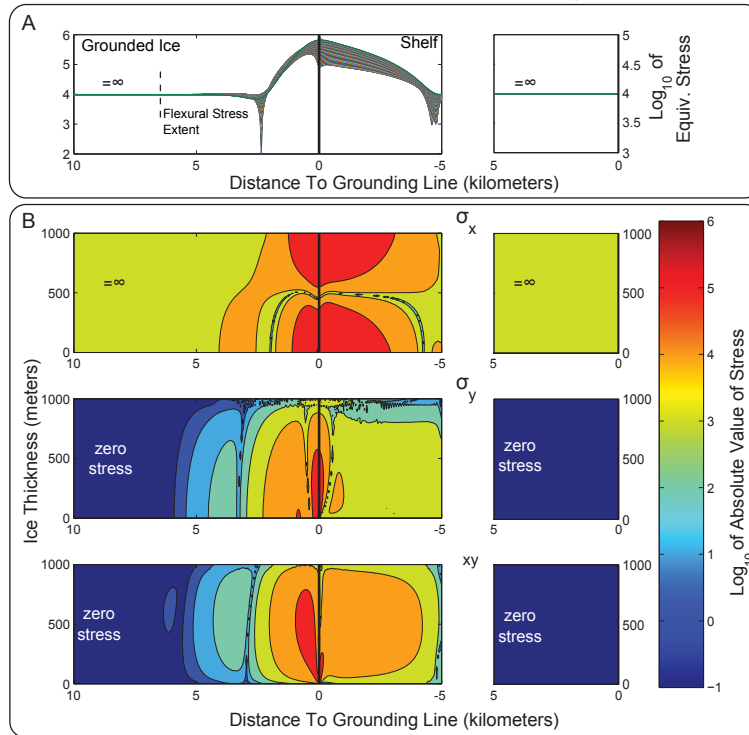


Fig. 3. Distributions of stress for a two-dimensional model with frictionless basal sliding. **(A)** Shows profiles of longitudinal σ_{eq} profiles at a depth interval of 10 m, while **(B)** shows the logarithm of the absolute value of the three in-plane stress components (σ_x , σ_y , and σ_{xy}) for the entire two-dimensional model domain. The left column for both panels shows a model with an ice shelf; the right column for both panels shows a model with no ice shelf and only an axial loading. In these frictionless models, axial stress does not decay with distance and flexural stress rapidly decays near the grounding line. L_{tr} is the stress decay length, and is defined in the main text.

Modeling the elastic transmission of tidal stresses to great distances

J. Thompson et al.

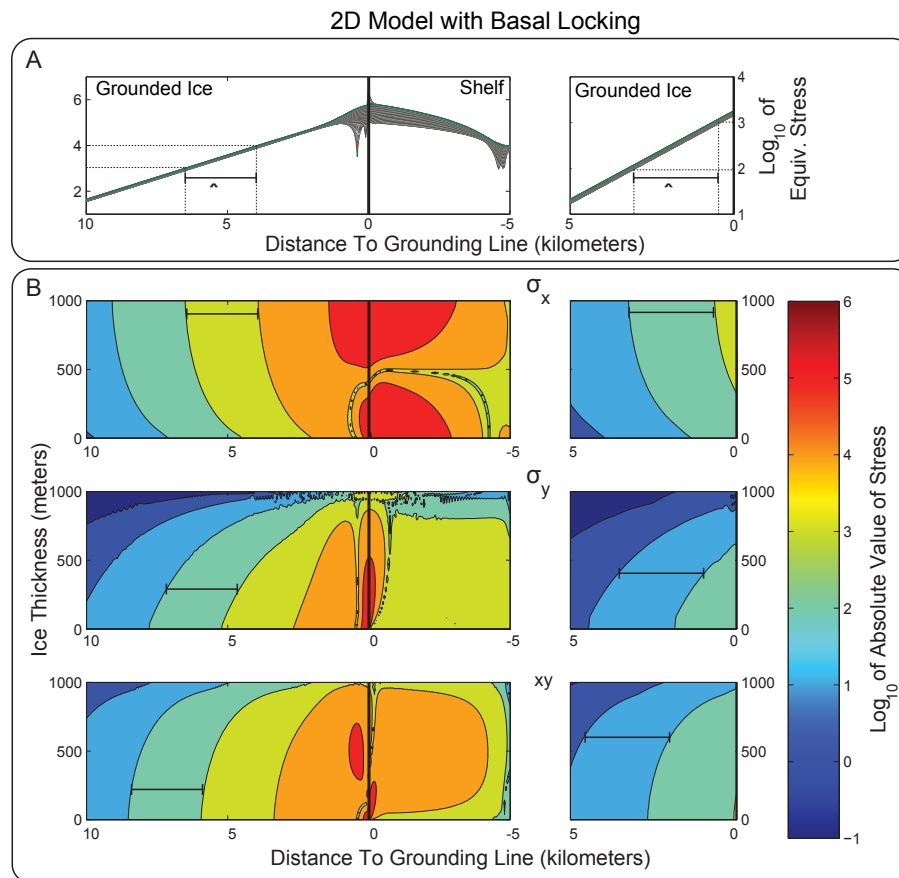


Fig. 4. Stress distributions for a two-dimensional model with no basal sliding. The panels are the same as in Fig. 3. Stress at the grounding line is higher in the model with an ice shelf than without a shelf, but L_r is the same between the two model setups.

Modeling the elastic transmission of tidal stresses to great distances

J. Thompson et al.

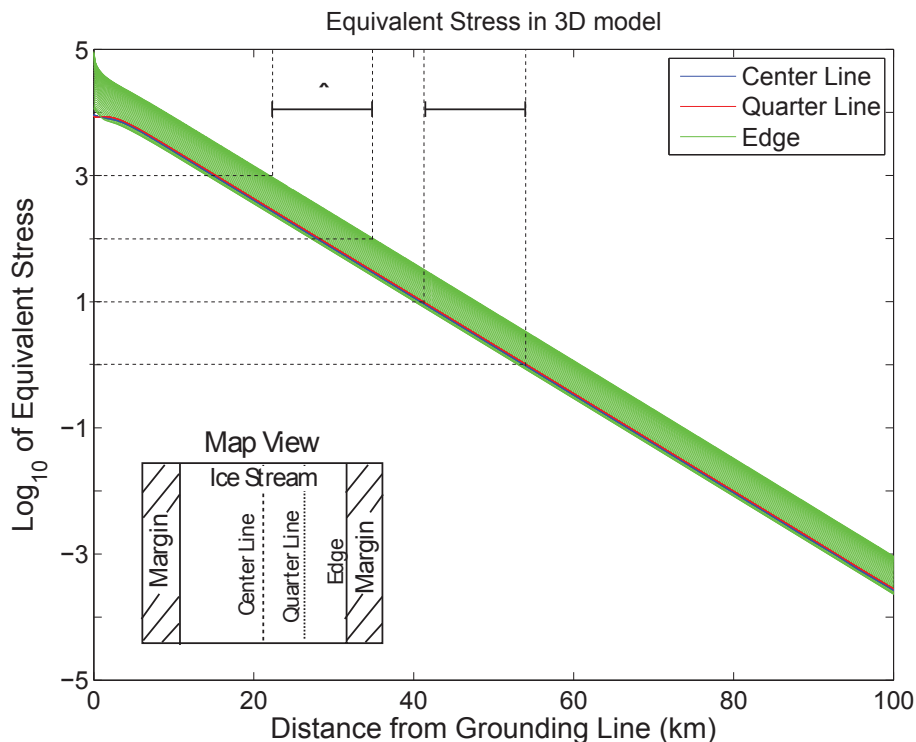


Fig. 5. Stacked equivalent stress (σ_{eq}) profiles for three different locations in a three-dimensional model with uniform elasticity, a width of 10 km, and a thickness of 1 km. The inset shows the locations of the three profiles in map view. For each location, 101 lines are stacked, taken at 10 m depth intervals. For the center and quarter lines, there is very little difference in stress value with depth, while for the edge of the ice stream, the stress value changes with depth by about an order of magnitude. However, between all these L_{tr} is constant.

Modeling the elastic transmission of tidal stresses to great distances

J. Thompson et al.

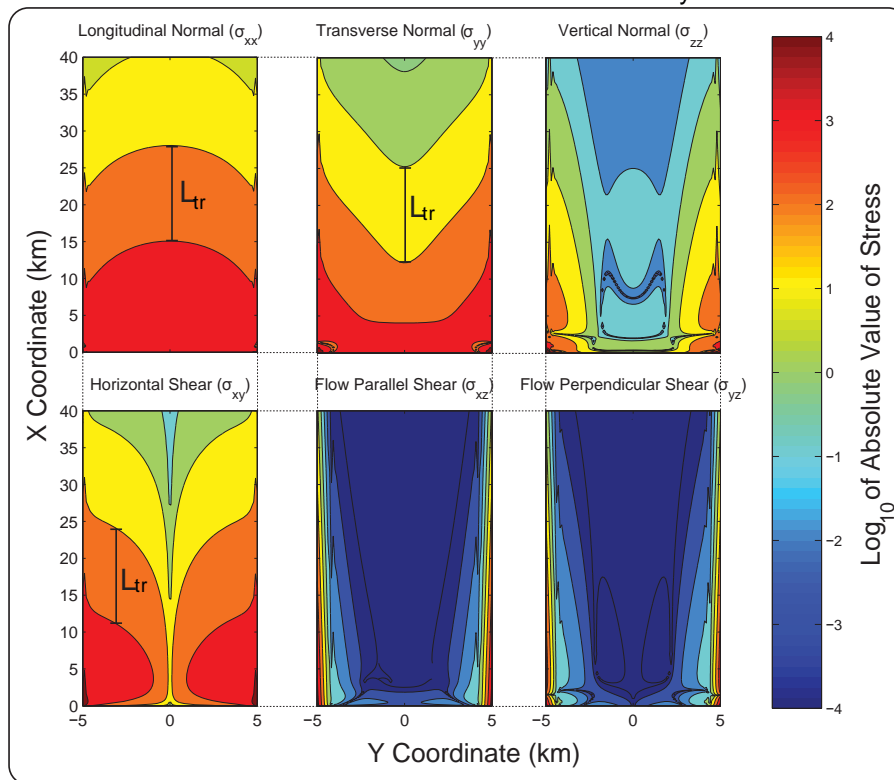


Fig. 6. Representative stress distribution along the base of a three-dimensional model with homogenous elasticity, showing the six unique stress components. The streaming portion of the model has a width of ten kilometers and a thickness of one kilometer. L_{tr} is drawn in the σ_{xx} , σ_{yy} , and σ_{xy} stress components where L_{tr} is easiest to observe.

Modeling the elastic transmission of tidal stresses to great distances

J. Thompson et al.

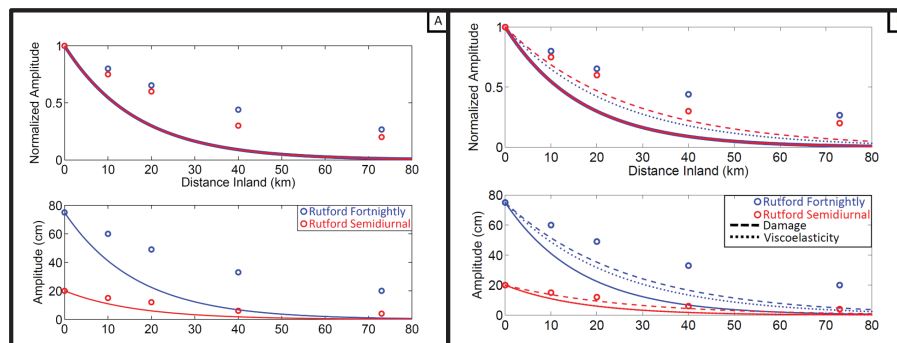


Fig. 7. Diagrams comparing GPS tidal displacement amplitudes to modeled displacement amplitudes. Circles show the data taken from observation on Rutford Ice Stream (Rutford data courtesy of H. Gudmundsson). The error on the approximated tidal displacement amplitudes is two centimeters. The slopes of the modeled surface displacements are taken from models approximating the Rutford Ice Stream, as shown in Table 5. The upper panel shows the distance-dependence of the equivalent stress calculated from linear, homogenous elastic model results, while (b) Shows the equivalent stress calculated using models accounting for elastic damage in the shear margins (dashed) and temperature-dependent viscoelasticity (dotted).

Title Page

Abstract

Introduction

Conclusions

References

Tables

Figures

⏪

⏩

◀

▶

Back

Close

Full Screen / Esc

Printer-friendly Version

Interactive Discussion

Modeling the elastic transmission of tidal stresses to great distances

J. Thompson et al.

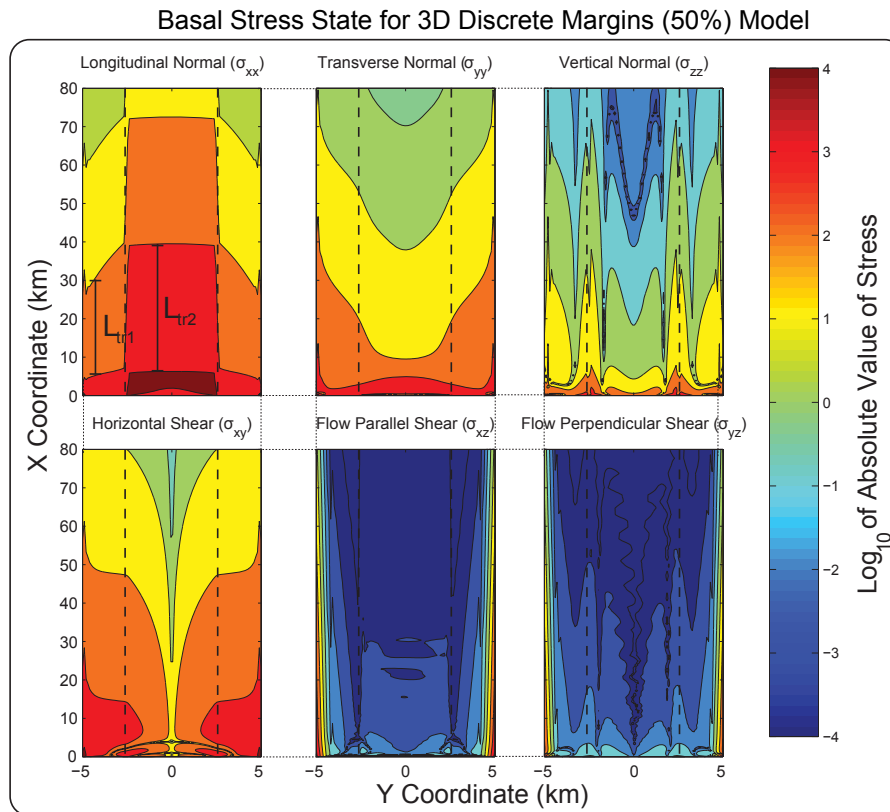


Fig. 8. Representative stress distribution for a model with the same geometry as Fig. 6, but with ice margins that are 1/4 the width of the ice stream. These margins are a factor of 10 more compliant than the central ice. A variable L_{tr} is highlighted in the σ_{xx} component of stress.

Title Page

Abstract

Introduction

Conclusions

References

Tables

Figures

◀

▶

◀

▶

Back

Close

Full Screen / Esc

Printer-friendly Version

Interactive Discussion

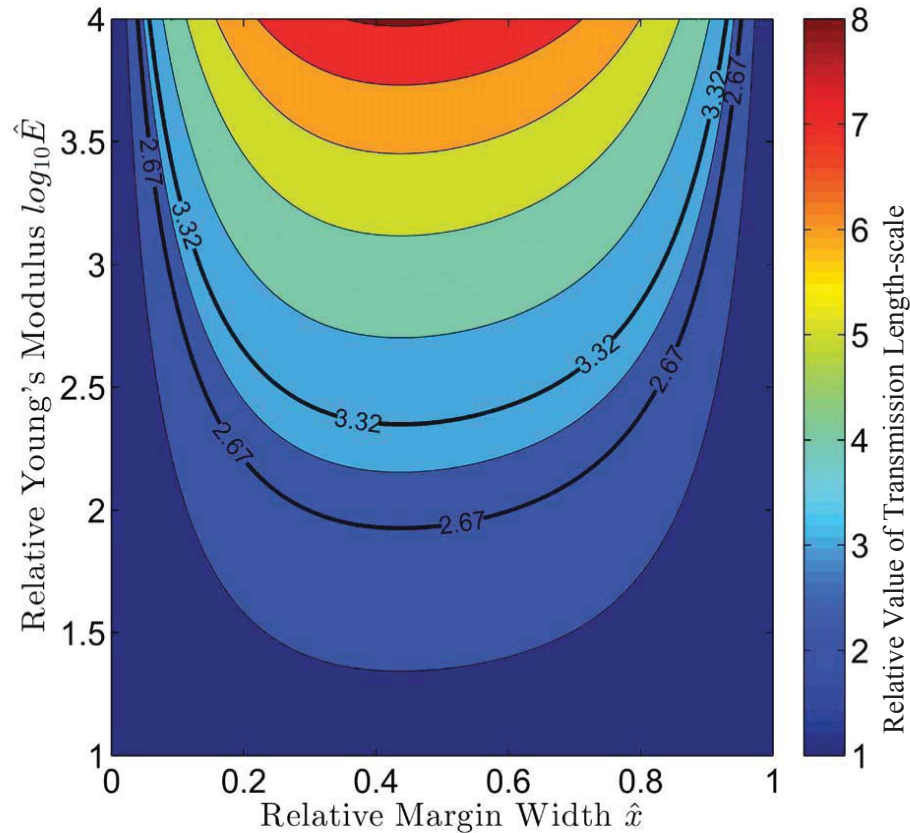


Fig. 9. Young's modulus and margin width space for the increase in L_{tr} for a discrete margin model relative to the homogeneous elastic model. The two bolded contours correspond to the conditions necessary to single-handedly explain the observations of the Rutherford fortnightly tidal signal (2.67) and the Rutherford semidiurnal tidal signal (3.32).

Modeling the elastic transmission of tidal stresses to great distances

J. Thompson et al.

Title Page

Abstract Introduction

Conclusions References

Tables Figures

⏪ ⏩

◀ ▶

Back Close

Full Screen / Esc

Printer-friendly Version

Interactive Discussion



Modeling the elastic transmission of tidal stresses to great distances

J. Thompson et al.

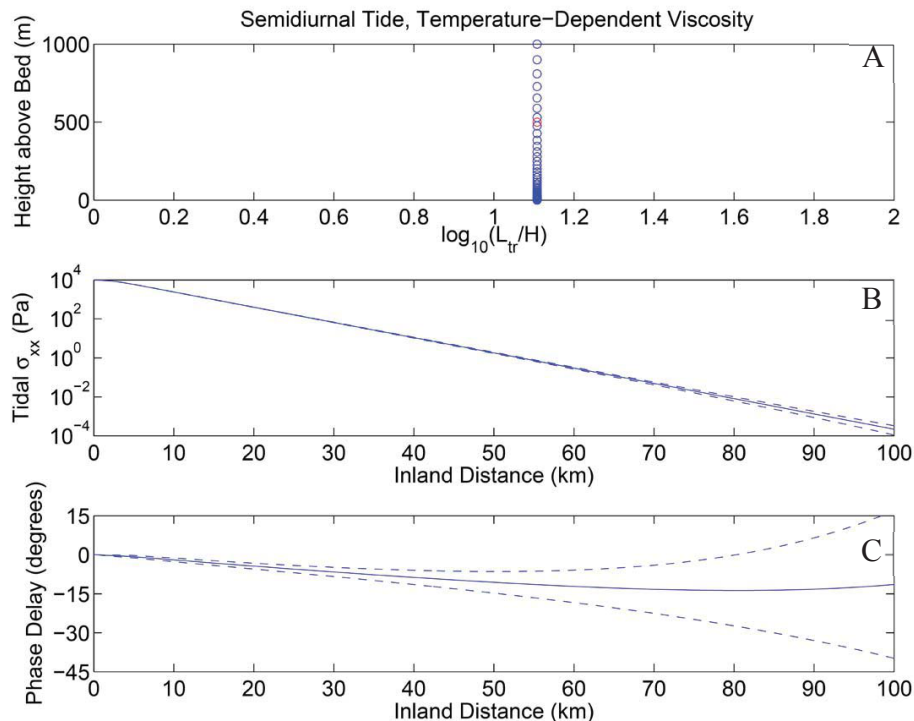


Fig. 10. Model results for a temperature-dependent viscoelastic model forced by a semidiurnal tide. **(A)** Shows the calculated values of L_{tr} for depth profiles of the stress. The average value of L_{tr} is 12.81 ± 0.001 km. **(B)** Shows the value of the longitudinal normal stress (σ_{yy}) as a function of horizontal coordinate. **(C)** Shows the fitted phase shift φ as a function of horizontal coordinate. In **(B and C)**, the dashed lines correspond to the 95 % confidence interval values of the fit.

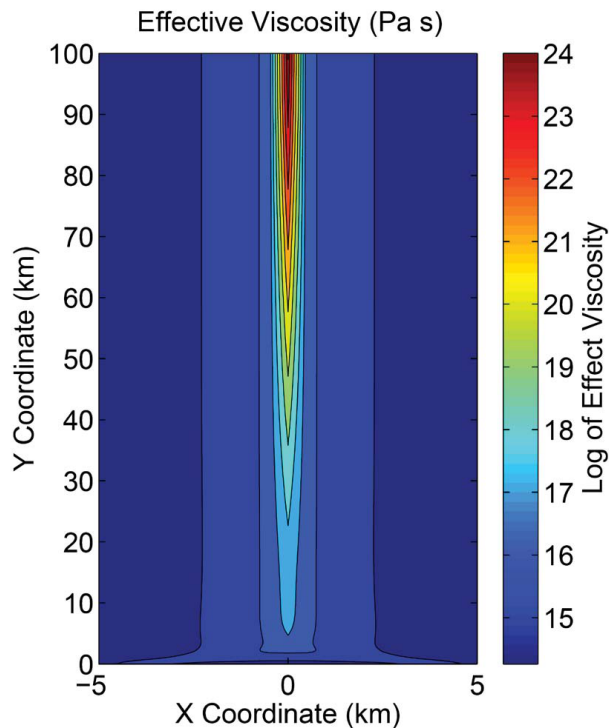


Fig. 11. Figure showing the basal effective viscosity of semidiurnal models for the homogeneous viscosity model. This figure demonstrates that the shear margins have substantially reduced viscosity relative to the central ice.

Modeling the elastic transmission of tidal stresses to great distances

J. Thompson et al.

Title Page

Abstract Introduction

Conclusions References

Tables Figures

⏪ ⏩

⏴ ⏵

Back Close

Full Screen / Esc

Printer-friendly Version

Interactive Discussion



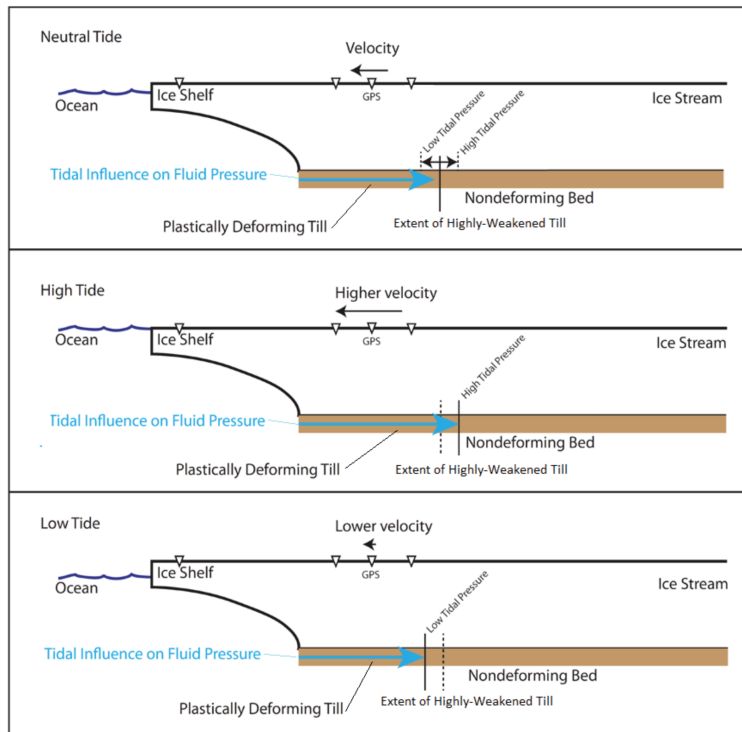


Fig. 12. Schematic view of our hydrology hypothesis at neutral, high, and low tidal amplitudes, respectively. The triangles represent GPS stations on the surface of the ice stream and ice shelf. The brown layer represents the subglacial till. Maximum extent of highly-weakened till is shown as a vertical line, and should vary in position with changes in the ocean tidal amplitude. Then the maximum extent of highly-weakened till is farther inland, the GPS stations move faster relative to a neutral position as more of the ice is streaming. Furthermore, when the maximum extent of highly-weakened till is closer to the grounding line, the relative velocity of the GPS stations is smaller than at a neutral tide.

Modeling the elastic transmission of tidal stresses to great distances

J. Thompson et al.

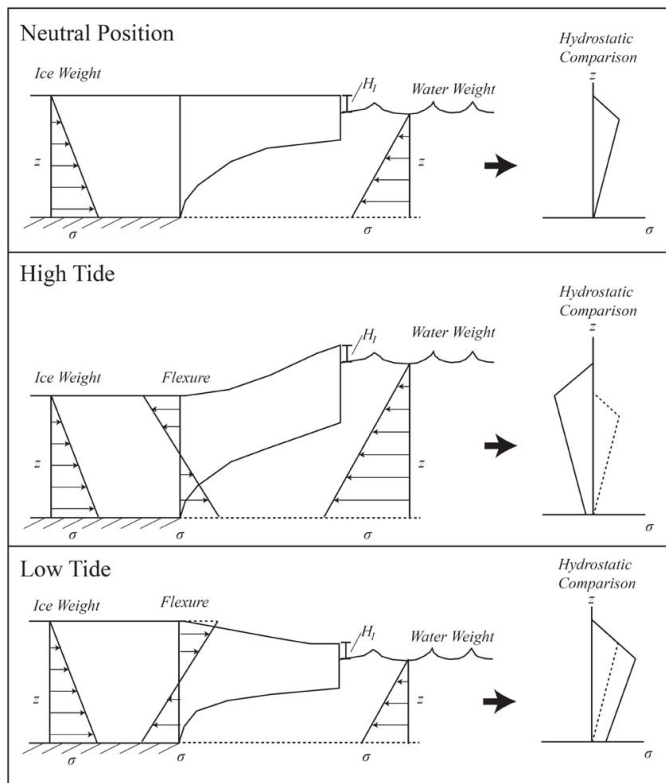


Fig. B1. Schematic diagrams of the full tidal forcing condition at a neutral, high, and low tide. The tidal stress will be the extensional/compressional stress due to the different in hydrostatic pressure at the edge of the ice shelf (shown in the graph on the right of the figure) and the flexural stresses due to the presence of the ice shelf. H_1 is the distance between the surface of the ice shelf and the surface of the ocean.

Modeling the elastic transmission of tidal stresses to great distances

J. Thompson et al.

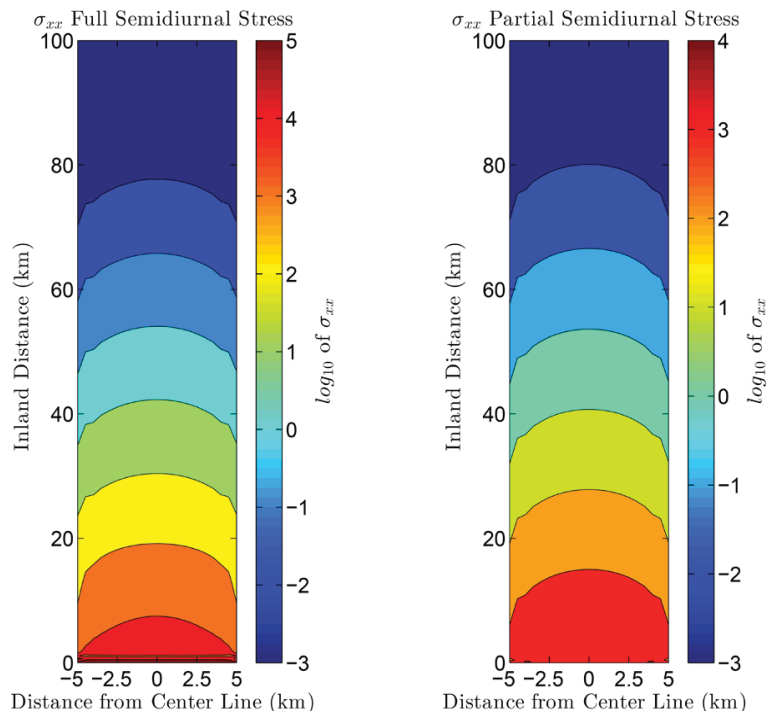


Fig. B2. Comparison of the value of the longitudinal normal stress (σ_{xx}) for the full tidal forcing condition (left) and the partial tidal forcing condition (right) at peak tidal amplitude. The full condition has a higher normal stress at the grounding line and a slightly more rapid decay of the stress due to the inclusion of the flexural stress. Once inland of the grounding line by five to ten kilometers, the stress-transmission length-scales are comparable between the two forcing conditions.

[Title Page](#)
[Abstract](#)
[Introduction](#)
[Conclusions](#)
[References](#)
[Tables](#)
[Figures](#)
[Back](#)
[Close](#)
[Full Screen / Esc](#)
[Printer-friendly Version](#)
[Interactive Discussion](#)

Modeling the elastic transmission of tidal stresses to great distances

J. Thompson et al.

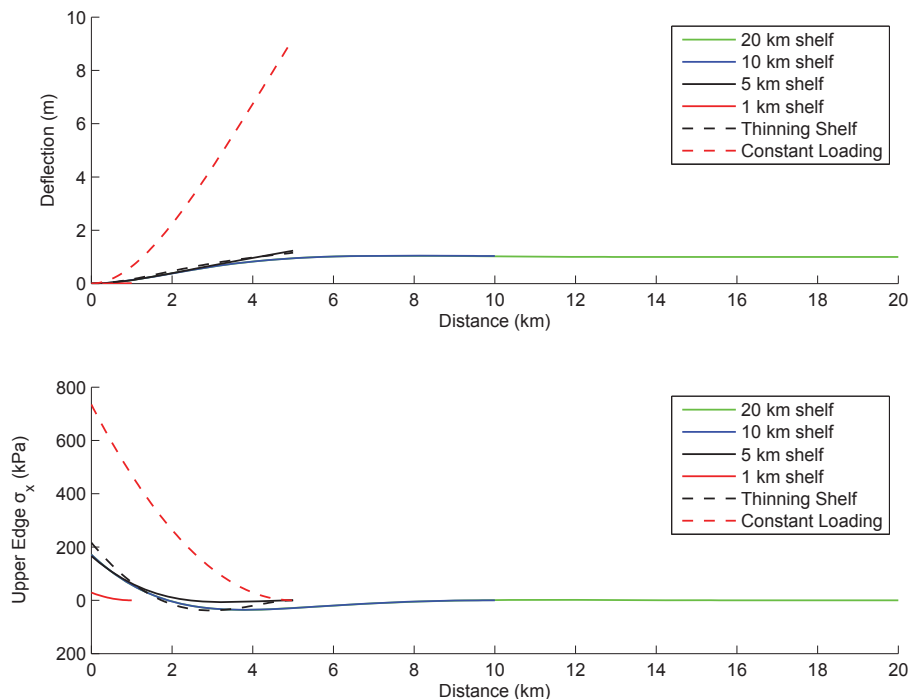


Fig. C1. Results of the 1-D flexural beam approximation of a floating ice shelf. The upper figure shows the beam deflection while the lower section shows the stress at the upper edge of the beam. See text in appendix C for a description of the governing equations and boundary conditions for the models shown.